References

1. Matsuoka M, Jeang KT (2007) Human T-cell leukaemia virus type 1 (HTLV-1) infectivity and cellular transformation. Nat Rev Cancer 7: 270–280.
2. Gessain A, Jouannelle A, Escarmant P, Calender A, Schaffar-Deshayes L, et al. (1984) HTLV antibodies in patients with non-Hodgkin lymphomas in Martinique. Lancet 1: 1183–1184.
3. Osame M, Usuku K, Izumo S, Ijichi N, Amitani H, et al. (1986) HTLV-I associated myelopathy, a new clinical entity. Lancet 1: 1031–1032.
4. Nakao K, Ohba N, Matsumoto M (1989) Noninfectious anterior uveitis in patients infected with human T-lymphotropic virus type I. Jpn J Ophthalmol 33: 472–481.
5. Mochizuki M, Yamaguchi K, Takatsuki K, Watanabe T, Mori S, et al. (1992) HTLV-I and uveitis. Lancet 339: 1110.
6. Sugimoto M, Nakashima H, Watanabe S, Uyama E, Tanaka F, et al. (1987) T-lymphocyte alveolitis in HTLV-I-associated myelopathy. Lancet 2: 1220.
7. LaGrenade L, Hanchard B, Fletcher V, Cranston B, Blattner W (1990) Infective dermatitis of Jamaican children: a marker for HTLV-I infection. Lancet 336: 1345–1347.
8. Morgan OS, Rodgers-Johnson P, Mora C, Char G (1989) HTLV-1 and polymyositis in Jamaica. Lancet 2: 1184–1187.
9. Matsuura E, Yamano Y, Jacobson S (2010) Neuroimmunity of HTLV-I Infection. J Neuroimmune Pharmacol 5: 310–325.
10. Satou Y, Yasunaga J, Yoshida M, Matsuoka M (2006) HTLV-I basic leucine zipper factor gene mRNA supports proliferation of adult T cell leukemia cells. Proc Natl Acad Sci U S A 103: 720–725.
11. Arnold J, Zimmerman B, Li M, Lairmore MD, Green PL (2008) Human T-cell leukemia virus type-1 antisense-encoded gene, Hbz, promotes T-lymphocyte proliferation. Blood 112: 3788–3797.
12. Satou Y, Yasunaga J, Zhao T, Yoshida M, Miyazato P, et al. (2011) HTLV-1 bZIP Factor Induces T-Cell Lymphoma and Systemic Inflammation In Vivo. PLoS Pathog 7: e1001274.
13. Zhao T, Satou Y, Sugata K, Miyazato P, Green PL, et al. (2011) HTLV-1 bZIP factor enhances TGF-{beta} signaling through p300 coactivator. Blood 118: 1865–1876.
14. Sakaguchi S, Yamaguchi T, Nomura T, Ono M (2008) Regulatory T cells and immune tolerance. Cell 133: 775–787.
15. Gavin M, Rudensky A (2003) Control of immune homeostasis by naturally arising regulatory CD4+ T cells. Current opinion in immunology 15: 690–696.
16. Zhou X, Bailey-Bucktrout SL, Jeker LT, Penaranda C, Martinez-Llordella M, et al. (2009) Instability of the transcription factor Foxp3 leads to the generation of pathogenic memory T cells in vivo. Nature immunology 10: 1000–1007.
17. Miyao T, Floess S, Setoguchi R, Luche H, Fehling HJ, et al. (2012) Plasticity of foxp3(+) T cells reflects promiscuous foxp3 expression in conventional T cells but not reprogramming of regulatory T cells. Immunity 36: 262–275.
18. Rubtsov YP, Niec RE, Josefowicz S, Li L, Darce J, et al. (2010) Stability of the regulatory T cell lineage in vivo. Science 329: 1667–1671.
19. Hori S, Nomura T, Sakaguchi S (2003) Control of regulatory T cell development by the transcription factor Foxp3. Science 299: 1057–1061.
20. Thornton AM, Korty PE, Tran DQ, Wohlfert EA, Murray PE, et al. (2010) Expression of Helios, an Ikaros transcription factor family member, differentiates thymic-derived from peripherally induced Foxp3+ T regulatory cells. Journal of immunology 184: 3433–3441.
21. Himmel ME, MacDonald KG, Garcia RV, Steiner TS, Levings MK (2013) Helios+ and Helios- cells coexist within the natural FOXP3+ T regulatory cell subset in humans. J Immunol 190: 2001–2008.
22. Gottschalk RA, Corse E, Allison JP (2012) Expression of Helios in peripherally induced Foxp3+ regulatory T cells. J Immunol 188: 976–980.
23. Akimova T, Beier UH, Wang L, Levine MH, Hancock WW (2011) Helios expression is a marker of T cell activation and proliferation. PLoS One 6: e24226.
24. Zheng Y, Josefowicz S, Chaudhry A, Peng XP, Forbush K, et al. (2010) Role of conserved non-coding DNA elements in the Foxp3 gene in regulatory T-cell fate. Nature 463: 808–812.
25. O'Shea JJ, Paul WE (2010) Mechanisms underlying lineage commitment and plasticity of helper CD4+ T cells. Science 327: 1098–1102.
26. Virgin HW, Wherry EJ, Ahmed R (2009) Redefining chronic viral infection. Cell 138: 30–50.
27. Bangham CR, Osame M (2005) Cellular immune response to HTLV-1. Oncogene 24: 6035–6046.
28. Moritoyo T, Reinhart TA, Moritoyo H, Sato E, Izumo S, et al. (1996) Human T-lymphotropic virus type I-associated myelopathy and tax gene expression in CD4+ T lymphocytes. Annals of neurology 40: 84–90.
29. Kubota R, Soldan SS, Martin R, Jacobson S (2002) Selected cytotoxic T lymphocytes with high specificity for HTLV-I in cerebrospinal fluid from a HAM/TSP patient. Journal of neurovirology 8: 53–57.
30. Dao T, Holan V, Minowada J (1993) Multiple and heterogeneous patterns of cytokine production in 18 leukemia and in vitro transformed mature T cell lines reflect the individuality of human leukemias. International journal of hematology 57: 139–146.
31. Macnamara A, Rowan A, Hilburn S, Kadolsky U, Fujiwara H, et al. (2010) HLA class I binding of HBZ determines outcome in HTLV-1 infection. PLoS Pathog 6: e1001117.
32. Sun SC, Yamaoka S (2005) Activation of NF-kappaB by HTLV-I and implications for cell transformation. Oncogene 24: 5952–5964.
33. Zhao T, Yasunaga J, Satou Y, Nakao M, Takahashi M, et al. (2009) Human T-cell leukemia virus type 1 bZIP factor selectively suppresses the classical pathway of NF-kappaB. Blood 113: 2755–2764.
34. Arnulf B, Villemain A, Nicot C, Mordelet E, Charneau P, et al. (2002) Human T cell lymphotropic virus oncoprotein tax represses TGF-{beta}1 signaling in human T cells via c-Jun activation: a potential mechanism of HTLV-I leukemogenesis. Blood 100:4129–38.
35. Lee DK, Kim BC, Brady JN, Jeang KT, Kim SJ (2002) Human T-cell Lymphotropic Virus Type 1 Tax Inhibits Transforming Growth Factor-beta Signaling by Blocking the Association of Smad Proteins with Smad-binding Element. J Biol Chem 277: 33766–33775.
36. Sugata K, Satou Y, Yasunaga J, Hara H, Ohshima K, et al. (2012) HTLV-1 bZIP factor impairs cell-mediated immunity by suppressing production of Th1 cytokines. Blood 119: 434–444.
37. Yang XO, Nurieva R, Martinez GJ, Kang HS, Chung Y, et al. (2008) Molecular antagonism and plasticity of regulatory and inflammatory T cell programs. Immunity 29: 44–56.
38. Komatsu N, Mariotti-Ferrandiz ME, Wang Y, Malissen B, Waldmann H, et al. (2009) Heterogeneity of natural Foxp3+ T cells: a committed regulatory T-cell lineage and an uncommitted minor population retaining plasticity. Proc Natl Acad Sci U S A 106: 1903–1908.
39. Xu L, Kitani A, Fuss I, Strober W (2007) Cutting edge: regulatory T cells induce CD4+CD25-Foxp3- T cells or are self-induced to become Th17 cells in the absence of exogenous TGF-beta. Journal of immunology 178: 6725–6729.
40. Yamano Y, Araya N, Sato T, Utsunomiya A, Azakami K, et al. (2009) Abnormally high levels of virus-infected IFN-gamma+ CCR4+ CD4+ CD25+ T cells in a retrovirus-associated neuroinflammatory disorder. PLoS One 4: e6517.
41. Saito M, Matsuzaki T, Satou Y, Yasunaga J, Saito K, et al. (2009) In vivo expression of the HBZ gene of HTLV-1 correlates with proviral load, inflammatory markers and disease severity in HTLV-1 associated myelopathy/tropical spastic paraparesis (HAM/TSP). Retrovirology 6: 19.
42. Karube K, Ohshima K, Tsuchiya T, Yamaguchi T, Kawano R, et al. (2004) Expression of FoxP3, a key molecule in CD4CD25 regulatory T cells, in adult T-cell leukaemia/lymphoma cells. Br J Haematol 126: 81–84.
43. Chen S, Ishii N, Ine S, Ikeda S, Fujimura T, et al. (2006) Regulatory T cell-like activity of Foxp3+ adult T cell leukemia cells. Int Immunol 18: 269–277.
44. Miyara M, Yoshioka Y, Kitoh A, Shima T, Wing K, et al. (2009) Functional delineation and differentiation dynamics of human CD4+ T cells expressing the FoxP3 transcription factor. Immunity 30: 899–911.
45. Satou Y, Utsunomiya A, Tanabe J, Nakagawa M, Nosaka K, et al. (2012) HTLV-1 modulates the frequency and phenotype of FoxP3+CD4+ T cells in virus-infected individuals. Retrovirology 9: 46.
46. Curotto de Lafaille MA, Lafaille JJ (2009) Natural and adaptive foxp3+ regulatory T cells: more of the same or a division of labor? Immunity 30: 626–635.
47. Kinashi T, Katagiri K (2005) Regulation of immune cell adhesion and migration by regulator of adhesion and cell polarization enriched in lymphoid tissues. Immunology 116: 164–171.

Regular Article

LYMPHOID NEOPLASIA

An animal model of adult T-cell leukemia: humanized mice with HTLV-1–specific immunity

Kenta Tezuka, Runze Xun, Mami Tei, Takaharu Ueno, Masakazu Tanaka, Norihiro Takenouchi, and Jun-ichi Fujisawa

Department of Microbiology, Kansai Medical University, Hirakata, Osaka, Japan

Key Points

- Humanized mice, IBMI-huNOG, were generated by intra–bone marrow injection of human CD133$^+$ hematopoietic stem cells.
- HTLV-1–infected IBMI-huNOG mice recapitulated distinct ATL-like symptoms as well as HTLV-1–specific adaptive immune responses.

Human T-cell leukemia virus type 1 (HTLV-1) is causally associated with adult T-cell leukemia (ATL), an aggressive T-cell malignancy with a poor prognosis. To elucidate ATL pathogenesis in vivo, a variety of animal models have been established; however, the mechanisms driving this disorder remain poorly understood due to deficiencies in each of these animal models. Here, we report a novel HTLV-1–infected humanized mouse model generated by intra–bone marrow injection of human CD133$^+$ stem cells into NOD/Shi-scid/IL-2Rγc null (NOG) mice (IBMI-huNOG mice). Upon infection, the number of CD4$^+$ human T cells in the periphery increased rapidly, and atypical lymphocytes with lobulated nuclei resembling ATL-specific flower cells were observed 4 to 5 months after infection. Proliferation was seen in both CD25$^-$ and CD25$^+$ CD4 T cells with identical proviral integration sites; however, a limited number of CD25$^+$-infected T-cell clones eventually dominated, indicating an association between clonal selection of infected T cells and expression of CD25. Additionally, HTLV-1–specific adaptive immune responses were induced in infected mice and might be involved in the control of HTLV-1–infected cells. Thus, the HTLV-1–infected IBMI-huNOG mouse model successfully recapitulated the development of ATL and may serve as an important tool for investigating in vivo mechanisms of ATL leukemogenesis and evaluating anti-ATL drug and vaccine candidates. (*Blood*. 2014;123(3):346-355)

Introduction

Human T-cell leukemia virus type 1 (HTLV-1) is a retrovirus associated with adult T-cell leukemia (ATL) and HTLV-1–associated myelopathy or tropical spastic paraparesis (HAM/TSP) in humans.[1-3] Although the majority of HTLV-1–infected individuals remain asymptomatic throughout their lives, approximately 5% of HTLV-1 carriers develop ATL or HAM/TSP following a long latency period.[4] In addition to the classic structural proteins required for retroviral replication, the HTLV-1 proviral genome encodes several accessory and regulatory proteins, including the viral transcriptional activator Tax and the HTLV-1 bZIP factor (HBZ), which are thought to be linked to HTLV-1 pathogenesis.[5,6]

ATL is an aggressive malignancy of mature CD4 T cells, characterized by frequent visceral involvement, lymphadenopathy, hypercalcemia or hypercytokinemia, and monoclonal proliferation of HTLV-1–infected tumor cells.[7] Typical ATL cells exhibit an unusual morphology with lobulated nuclei, known as "flower cells."[8] These cells are also characterized by their robust expression of interleukin (IL)-2 receptor α (CD25).[9]

To reproduce the pathogenesis of ATL, a number of mouse models have been developed, including transgenic or xenografted/humanized mice.[10-18] One such model is the Tax-transgenic mouse, which expresses Tax under the control of the Lck promoter. This model restricts Tax expression to developing thymocytes, resulting in characteristic ATL-like phenotypes.[15] Another model, the HBZ-transgenic mouse, expresses HBZ under the control of a CD4-specific promoter/enhancer/silencer. These mice develop lymphomas characterized by induction of Foxp3 in CD4 T cells, similar to leukemic cells in ATL patients.[18] These observations clearly demonstrate that the leukemogenic activity of not only Tax but also HBZ is related to the development of ATL.

In addition to transgenic mouse models, a variety of HTLV-1–infected small-animal models have been established to evaluate viral pathogenesis and elucidate the function of viral products in vivo.[19,20] These infection models have provided valuable findings regarding virus-host interactions; however, they are unable to fully recapitulate pathological conditions resembling ATL, likely due to the low efficiency of HTLV-1 infection.

Humanized mice are highly susceptible to infection with human lymphotropic viruses such as EBV, HIV-1, and HTLV-1, and have been used to recapitulate specific disorders and human immune responses.[17,21,22] Recent studies on HTLV-1 infection in humanized mouse models successfully reproduced HTLV-1–associated T-cell lymphomas[16,17]; however, these models did not accurately recreate human immune responses against HTLV-1.

Submitted June 17, 2013; accepted October 27, 2013. Prepublished online as *Blood* First Edition paper, November 6, 2013; DOI 10.1182/blood-2013-06-508861.

The online version of this article contains a data supplement.

There is an Inside *Blood* commentary on this article in this issue.

The publication costs of this article were defrayed in part by page charge payment. Therefore, and solely to indicate this fact, this article is hereby marked "advertisement" in accordance with 18 USC section 1734.

Notably, humoral immunity, along with cytotoxic T cell (CTL)-mediated cytotoxicity, is thought to play a pivotal role in controlling the proliferation or selection of HTLV-1–infected T-cell clones in vivo.[23,24] It is therefore important to develop mouse models of ATL that induce more human-like HTLV-1–specific immune responses.

In this study, we describe a novel humanized mouse model of HTLV-1 infection in the presence of specific adaptive immune responses. Our novel HTLV-1–infected humanized mice displayed distinct ATL-like symptoms, including hepatosplenomegaly, hypercytokinemia, oligoclonal proliferation of HTLV-1–infected T cells, and the appearance of flower cells. In addition, HTLV-1–specific immunity was induced and may be involved in the control of infected cells in vivo.

Materials and methods

Purification of human CD133$^+$ cells from cord blood

Cord blood samples from full-term human deliveries were obtained from the Japanese Red Cross Kinki Cord Blood Bank (Osaka, Japan) for research use due to the inadequate numbers of stem cells for human transplantation; all patients provided signed, informed consent in accordance with the Declaration of Helsinki. Mononuclear cells (MNCs) were separated using Ficoll-Conray (Lymphosepar I, IBL) density gradient centrifugation. After collecting MNCs, a CD133 MicroBead Kit (Miltenyi Biotec) was used to isolate human CD133$^+$ cells (Miltenyi Biotec) according to the manufacturer's instructions. HLA-A typing was performed using a WAKFlow HLA typing kit (WAKUNAGA) according to the manufacturer's instructions; the results are shown in supplemental Table 1 (available on the *Blood* Web site).

NOG mice

Female 6-week-old NOD/Shi-scid/IL-2Rγc null (NOG) mice[25] were purchased from the Central Institute of Experimental Animals (Kawasaki, Japan). Mice were handled under sterile conditions and were maintained in germ-free isolators. All animal experiments were approved by the Animal Care Committees of Kansai Medical University.

Generation of IBMI-huNOG

Seven-week-old NOG mice were sublethally irradiated with 250 cGy from a ^{137}Cs source (Gammacell 40 exactor, Nordion International). Within 24 hours of irradiation, each mouse was injected with 5×10^4 human CD133$^+$ cells by intra–bone marrow injection (IBMI)[26] as reported previously.[27]

HTLV-1 infection to IBMI-huNOG

The HTLV-1–infected T-cell line MT2[28] was irradiated with 10 Gy from a ^{137}Cs source irradiator. Irradiated MT2 cells (2.5×10^6) or phosphate-buffered saline were inoculated intraperitoneally into 24- to 28-week-old IBMI-huNOG mice. Mice were anesthetized and killed when the body weight decreased to <70% of their maximum weight. Peripheral blood smears were prepared using May-Grunwald Giemsa staining and examined by light microscopy. All infections were performed in a Biosafety Level P2A laboratory in accordance with the guidelines of Kansai Medical University.

Flow cytometric analysis and cell sorting

Peripheral blood cells were routinely collected every 2 weeks after infection, and after sacrificing mice, single-cell suspensions of various lymphoid tissues were prepared as described previously.[29] To stain surface markers, anti–human CD45-PerCP or APC-Cy7, CD3–fluorescein isothiocyanate (FITC) or phycoerythrin (PE)-Cy7, CD4-PE, CD8-PerCP-Cy5.5, CD19-PE, CD25-FITC, CCR4-APC antibodies were used, along with mouse immunoglobllin G1 and FITC as an isotype control (all BD Biosciences). AccuCount Ultra Rainbow Fluorescent Particles (Spherotech) were employed to determine absolute cell numbers, according to the manufacturer's protocol. Flow cytometric analysis was performed on a BD FACSCan for 3-color staining and a BD FACSCant II (BD Biosciences) for 7-color staining. The CellQuest and Diva software programs were used for data acquisition (BD Biosciences), and the collected data were analyzed by FCS express 3 (De Novo Software). Human CD4-, CD8-, and CD25-expressing T cells were sorted from splenic MNCs by FACSAria or FACSAria III (BD Biosciences).

Tetramer staining

PE-conjugated HLA-A*24:02/Tax301-309 (SFHSLHLLF) and HLA-A*24:02/HIV (RYLRDQQLL) env gp160 tetramers were purchased from MBL. Splenocytes from mock-infected or HTLV-1–infected mice were stained with each tetramer and anti–human CD3 and CD8 antibodies according to the manufacturer's protocol. Mixed lymphocyte-peptide cultures were performed to stimulate Tax-specific CTLs, as described previously.[30] Briefly, splenocytes from HTLV-1–infected mice were cultured for 13 days with 10 mg/mL Tax301-309 peptide and 50 U/mL recombinant human IL-2 (Takeda Chemical Industries). Cultured splenocytes were then analyzed by flow cytometry.

DNA isolation and quantification of proviral load

Genomic DNA was extracted from single-cell suspensions of tissue or peripheral blood using a conventional phenol extraction method. Proviral loads (PVLs) were measured by quantitative polymerase chain reaction (PCR) using a MyiQ or CFX96 real-time PCR system (Bio-Rad). The primers and probes targeting for HTLV-1 *pX* and human β-globin (HBB; as a internal control) are listed in supplemental Table 2. A plasmid containing PCR fragments for the HTLV-1 *pX* region and HBB was constructed using T-Vector pMD20 (TaKaRa) and used as the quantified standard template for real-time PCR.[31] The PVL was calculated as: [(copy number of *pX*)/(copy number of HBB / 2)] × 100.

Quantification of clonal occupancy by clone-specific PCR

Inverse long PCR (IL-PCR) was performed to amplify the genomic DNA flanked the 3′ long terminal repeat of HTLV-1 provirus according to a modified method described previously.[32] In brief, the genomic DNA was digested by *Pst*I, self-ligated by T4 ligase, and then digested by *Mlu*I. Long PCR amplification of the linearized DNA was performed using the PrimeSTAR GXL DNA polymerase (TaKaRa) according to the manufacturer's protocol. Primer sets for IL-PCR analysis are listed in supplemental Table 3. IL-PCR products were isolated from agarose gels, purified, and subjected to nested PCR. Amplified nested PCR fragments were subcloned into T-Vector pMD20 (TaKaRa) and sequenced to obtain provirus integration sites downstream of the 3′ long terminal repeat. Integration site-specific primers were designed based on the DNA sequence of the flanking region of the provirus derived from splenic DNA of 8 HTLV-1–infected mice, and are listed in supplemental Table 5. A detailed description of the clone-specific quantitative PCR procedure has been provided elsewhere.[33] The clonal occupancy of each clone was calculated as: [(copy number of integration sites)/(copy number of *pX*)] × 100.

Real-time RT-PCR to quantify *tax* and *HBZ* transcripts

Total RNA was isolated using the TRIzol reagent (Invitrogen) and complementary DNA samples were synthesized from 1 μg total RNA. Reverse-transcription PCR (RT-PCR) was performed by the use of SsoFast EvaGreen Supermix (Bio-Rad). Primers used for RT-PCR are listed in supplemental Table 4. Relative expression levels were calculated by the MyiQ system (Bio-Rad).

Titration of HTLV-1–specific antibodies

The titers of antibodies against HTLV-1 antigens in the plasma of infected mice were determined by the particle agglutination method using Serodia

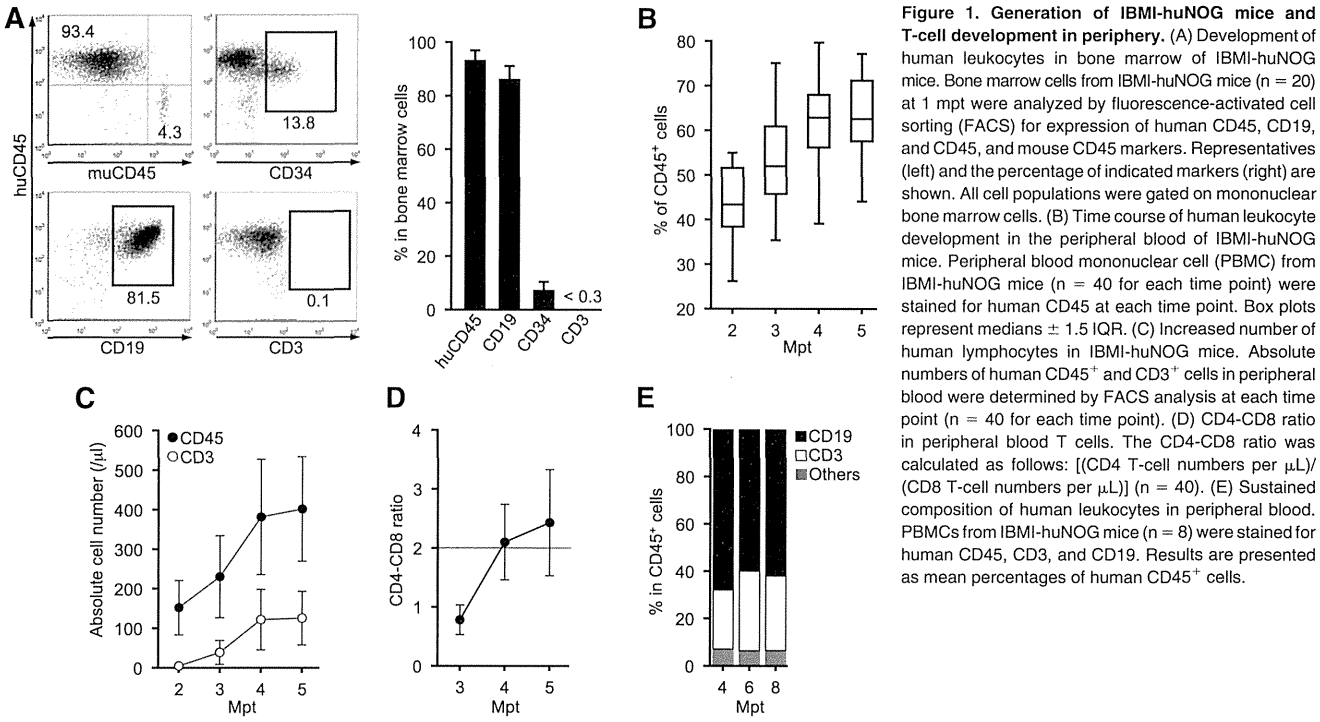

Figure 1. Generation of IBMI-huNOG mice and T-cell development in periphery. (A) Development of human leukocytes in bone marrow of IBMI-huNOG mice. Bone marrow cells from IBMI-huNOG mice (n = 20) at 1 mpt were analyzed by fluorescence-activated cell sorting (FACS) for expression of human CD45, CD19, and CD45, and mouse CD45 markers. Representatives (left) and the percentage of indicated markers (right) are shown. All cell populations were gated on mononuclear bone marrow cells. (B) Time course of human leukocyte development in the peripheral blood of IBMI-huNOG mice. Peripheral blood mononuclear cell (PBMC) from IBMI-huNOG mice (n = 40 for each time point) were stained for human CD45 at each time point. Box plots represent medians ± 1.5 IQR. (C) Increased number of human lymphocytes in IBMI-huNOG mice. Absolute numbers of human $CD45^+$ and $CD3^+$ cells in peripheral blood were determined by FACS analysis at each time point (n = 40 for each time point). (D) CD4-CD8 ratio in peripheral blood T cells. The CD4-CD8 ratio was calculated as follows: [(CD4 T-cell numbers per μL)/(CD8 T-cell numbers per μL)] (n = 40). (E) Sustained composition of human leukocytes in peripheral blood. PBMCs from IBMI-huNOG mice (n = 8) were stained for human CD45, CD3, and CD19. Results are presented as mean percentages of human $CD45^+$ cells.

HTLV-1 (Fuji Rebio).[23] To deplete human immunoglobulin M (IgM) or immunoglobulin G (IgG), streptavidin M-PVA magnetic beads (Chemagen) preincubated with biotin-conjugated goat anti–human IgM or IgG antibody (Sigma-Aldrich) were added to plasma from infected mice; a goat anti–mouse IgG antibody (Organon Teknika) was used as the negative control.

Bio-Plex cytokine assay

Plasma levels of IL-1b, IL-2, IL-4, IL-5, IL-6, IL-7, IL-8, IL-10, IL-12 (p70), IL-13, IL-17, granulocyte colony-stimulating factor (G-CSF), granulocyte macrophage colony-stimulating factor (GM-CSF), interferon-γ (IFN-γ), MCP-1, MIP-1β, and tumor necrosis factor α (TNF-α) in HTLV-1–infected and control mice were analyzed using the Bio-Plex Human Cytokine 17-Plex Panel (Bio-Rad) on a Bio-Plex 200 system according to the manufacturer's instructions.

Statistical analysis

The significance of differences was determined by Mann-Whitney *U* test, paired *t* test, or Spearman's rank-correlation coefficient (*r*); $P < .05$ was considered to indicate statistical significance.

Results

Reconstitution of human immune cells in NOG mice using IBMI

IBMI-huNOG mice were generated by IBMI of human $CD133^+$ hematopoietic stem cells into sublethally irradiated 6- to 7-week-old NOG mice. After 1 month of transplantation, human $CD45^+$ leukocytes were found to have almost completely reconstituted the bone marrow of recipient mice (Figure 1A). At this time point, the majority of the human leukocytes in bone marrow consisted of $CD19^+$ cells. A substantial number of $CD34^+$ cells were also detected, whereas human $CD3^+$ cells had not developed.

Less than half of peripheral blood cells were composed of human leukocytes even at 2 months posttransplantation (mpt). However, the number of human leukocytes increased in a time-dependent manner (Figure 1B-C). Between 3 and 4 mpt, the number of human $CD3^+$ T cells in the peripheral blood increased dramatically, as did the CD4-CD8 ratio (Figure 1D). $CD3^+$ T cells and the CD4-CD8 ratio reached stable levels by 4 to 5 mpt, suggesting that the development of human T cells was completed within this period.

Previous reports have shown that reconstituted human $CD45^+$ cells in other types of humanized mouse systems were overcome by $CD3^+$ T cells within several months of transplantation due to the reduction of B-cell development,[21,34] which may impair the integrity of host immunity. In contrast, the IBMI-huNOG mice model maintained a stable number of $CD3^+$ T cells as well as the B- to T-cell ratio in peripheral blood through at least 8 mpt (Figure 1E). Thus, the human immune system appeared to be effectively reconstituted in IBMI-huNOG mice, likely due to the enriched repopulation of long-term hematopoietic stem cells by direct injection of $CD133^+$ cells into the bone marrow cavity.[27]

Proliferation of HTLV-1–infected T cells in IBMI-huNOG mice

Human T lymphocytes fully developed in IBMI-huNOG mice within 4 to 5 mpt. These mice were then infected with HTLV-1 by intraperitoneal inoculation with 2.5×10^6 irradiated MT2 cells. The number of human $CD45^+$ leukocytes began to increase as early as 4 to 6 weeks postinoculation (wpi) and continued to increase rapidly thereafter (Figure 2A). HTLV-1 infection was also detected by 2 wpi, with the HTLV-1 PVL in peripheral blood increasing in a time-dependent manner (Figure 2B). The proportion of $CD3^+/CD45^+$ T lymphocytes was significantly enriched in HTLV-1–infected mice relative to mock-infected controls (Figure 2C), consistent with previous results.[16] Absence of residual MT2 cells used as the source of HTLV-1 was confirmed by MT2 cell-specific PCR as previously described (supplemental Figure 1).[35]

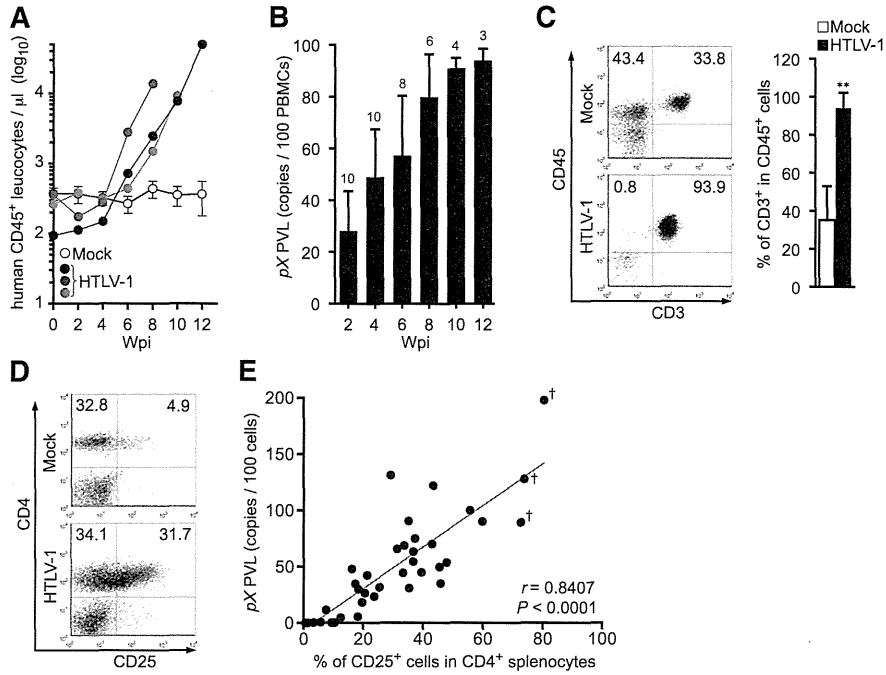

Figure 2. Kinetic analysis of HTLV-1 provirus in infected IBMI-huNOG mice. (A) Quantification of leukocyte numbers in the peripheral blood of HTLV-1–infected mice. Peripheral blood was routinely collected from mock- and HTLV-1–infected mice every 2 weeks. Human CD45$^+$ leukocytes were enumerated by FACS. Results from mock-infected mice (n = 10) are presented as mean ± standard deviation (SD), and representative results of 3 HTLV-1–infected mice are shown. (B) Quantification of HTLV-1 PVL in the peripheral blood of HTLV-1–infected mice. The PVL was determined by real-time PCR. Number at the top of each bar represents the number of analyzed HTLV-1–infected mice at each time point. (C) Expansion of CD3$^+$ T-cell populations in the peripheral blood of HTLV-1–infected mice. PBMCs from mock-infected (n = 3) and HTLV-1–infected mice (n = 18) were stained for human CD3 when sacrificed; the median value was 8 wpi. Results are presented as the average percentages ± SD of human CD45$^+$ cells. (D) Expansion of CD25$^+$ CD4 T cells in the spleen of HTLV-1–infected mice. Splenocytes were stained for human CD3, CD4, and CD25 and analyzed by FACS. Representative results from mock-infected (mouse ID: 8X20) and HTLV-1–infected (mouse ID: 8X01) mice are shown. (E) Correlation between the percentages of CD25$^+$ T cells and PVLs in the spleen. HTLV-1–infected mice (n = 37) were sacrificed to determine PVL and CD25$^+$ T-cell frequency in CD4$^+$ splenocytes. One dot represents the result of an individual HTLV-1–infected mouse. Spearman's rank-correlation coefficient (r) was adopted to identify statistically significant correlations between values. Daggers indicate that flower cells were observed in the peripheral blood of HTLV-1–infected mice.

HTLV-1–infected humanized mice showed marked expansion of CD25$^+$ CD4 T cells in the spleen relative to mock-infected controls (Figure 2D; Table 1), as is observed in peripheral blood of ATL and HAM/TSP patients.[9,36] Furthermore, PVLs in the spleen were significantly correlated with the rate of CD25$^+$ CD4 T cells (Figure 2E). These data suggest that the expanded CD25$^+$ CD4 T-cell population represents the majority of HTLV-1–infected cells in vivo.

ATL-like leukemic symptoms in HTLV-1–infected IBMI-huNOG mice

The majority of HTLV-1–infected mice exhibited splenomegaly, while apparent infiltration of infected T cells in the liver was observed in 3 infected mice with flower cells (Figure 3A; Table 1) and the weight of liver in these mice was remarkably increased (HTLV-1: 1550 ± 620 mg [n = 3]; mock: 715 ± 85 mg [n = 3]). When PVLs of several lymphoid organs were analyzed, the proportions of infected cells in the bone marrow and lymph nodes were significantly lower than those in the spleen and peripheral blood, consistent with the leukemic phenotype of infected mice (Figure 3B). This result is in striking contrast to other humanized mouse models, in which HTLV-1 infection[17] or the ectopic expression of Tax[16] preferentially induce lymphoma.

May-Grunwald Giemsa staining of peripheral blood smears from infected mice revealed the presence of large, abnormal leukemic cells with lobulated nuclei, which were morphologically identical to the flower cells observed in ATL patients (Figure 3D-E).[8] The activated phenotype of infected T cells was also evident, with clear downregulation of CD3 expression on the surface of peripheral T cells in HTLV-1–infected mice, similar to that seen in ATL cells (Figure 3C).[37]

ATL cells have been shown to secrete proinflammatory cytokines, such as IL-6, TNF-α, and GM-CSF, which stimulate activation and proliferation of infected T cells and promote development of ATL leukemogenesis.[38-40] Analysis of cytokine and chemokine levels in the plasma of HTLV-1–infected mice revealed significantly elevated levels of several proinflammatory cytokines (Figure 4). The concentration of IFNγ significantly correlated with PVL in the peripheral blood (supplemental Figure 2), suggesting Th1 immune responses induced in infected mice. Together, these results suggest that HTLV-1–infected IBMI-huNOG mice accurately recreate many of the pathological features of ATL, including hepatosplenomegaly, leukemic T-cell overgrowth with lobulated nuclei, hypercytokinemia, and downregulation of CD3 on T cells.

Oligoclonal proliferation of human T-cell clones in HTLV-1–infected IBMI-huNOG mice

To evaluate the clonal proliferation of HTLV-1–infected T cells in infected mice, we quantified cellular clonality using clone-specific real-time PCR analysis. Splenocytes were isolated from 8 infected mice sacrificed at various time points, and genomic DNA fragments

Table 1. Pathological features of mock- or HTLV-1–infected IBMI-huNOG mice

Mouse ID*	Wpi†	PVL‡	$CD3^+CD4^+$ (%)§	$CD4^+CD25^+$ (%)§	Spleen weight (mg)	Lymph node weight (mg)‖	Observations
8807	—	—	16.7	2.6	45	1	Mock infected
8X10	—	—	20.2	3.4	51	3	Mock infected
8X20	—	—	36.5	4.4	40	2	Mock infected
8401	17	65.6	53.1	31.4	195	23	
8402	11	0.1	5.3	0.7	26	1	
8403	14	0.1	10.8	3.4	35	1	
8404	17	5.4	53.4	18.3	68	2	
8405	12	11.3	30.3	7.6	59	14	
8406	5	0.1	10.5	1.5	33	3	
8407	8	4.5	69.6	12.5	166	9	
8801	25	0.1	59.6	10.4	187	7	
8803	30	0.4	38.6	5.8	55	11	
8804	23	0.1	46.6	9.5	105	5	
8805	8	70.0	57.0	43.1	233	37	Leukemia
8808	8	26.5	52.5	20.6	101	40	
8810	4	42.2	55.4	21.3	40	22	
8X01	5	44.9	65.8	39.5	208	11	
8X04	8	121.9	62.2	43.5	165	7	Leukemia
8X05	23	127.7	81.4	73.9	226	8	Leukemia, flower cells (10.6%),¶ tumor lesion
8X06	9	31.6	50.5	25.5	155	5	
8X09	5	34.6	52.2	17.4	227	9	
8X12	4	47.9	58.5	16.2	188	11	
8X14	25	68.6	51.4	33.8	145	25	Leukemia
8X16	7	90.4	78.9	35.2	200	16	Leukemia
8X17#	9	131.1	44.6	29.3	200	35	Leukemia
8X18	18	197.7	89.4	80.5	358	28	Leukemia, flower cells (19.2%),¶ tumor lesion
9Z01	10	53.6	75.8	47.9	220	12	Leukemia
9Z03	6	23.4	51.6	23.7	38	18	
9Z17	6	18.2	64.7	19.7	163	10	
9Z18	16	89.2	80.4	72.7	285	5	Leukemia, flower cells (4.2%),¶ tumor lesion
9Z19	6	35.0	65.0	45.9	207	20	
X202	12	90.0	76.6	59.9	353	13	Leukemia
X206	8	54.4	56.6	36.7	317	15	
X207**	11	100.0	62.2	55.7	358	6	Leukemia
X208	4	29.9	74.7	18.4	188	15	
X209	7	30.8	74.4	35.4	270	21	
X212	9	74.9	56.8	37.4	270	5	Leukemia
X214	10	44.3	48.0	33.3	170	6	
X216	8	63.2	66.1	36.9	271	12	Leukemia
X217	7	49.6	76.9	45.5	306	18	Leukemia

Leukemia, infected mice with atypical lymphocytes >90% of PBMCs; flower cells, atypical lymphocytes with >4 lobulated nuclei in a cell; tumor lesion, tumor formation of infiltrating infected T cells in the liver.

*The 37 infected mice listed are identical to those in Figure 2E.

†The wpi when indicated mice were sacrificed.

‡PVL is expressed as number of *pX* copies per 100 cells.

§The population of indicated marker-positive cells in $CD45^+$ splenocytes.

‖The weight value of one of the largest mesenteric lymph node in each mouse.

¶The percentage of flower cells in total lymphocytes in blood smear (presented in parentheses).

#High proportion of $CD25^+$ CD8 T cells in PBMCs.

**High proportion of DP T cells in PBMCs.

flanking the major integration sites in the HTLV-1–infected cells were amplified by IL-PCR. Amplified DNA fragments were subcloned into plasmids and sequenced to confirm proper integration (supplemental Table 5). As shown in Figure 5A, the occupancy of detected clones determined by real-time PCR was < 5% in cells harvested 5 to 8 wpi, indicating polyclonal HTLV-1 infection in these mice. In contrast, 2 mice sacrificed after prolonged infection periods (18 and 23 wpi, respectively) produced high percentages of infected clones. Interestingly, these 2 mice also showed overgrowth of $CD25^+$ CD4 T cells with flower-shaped nuclei, characteristic of ATL cells (Figure 3D-E), whereas such cells were not observed in the 6 remaining mice. These findings indicate that a limited number of HTLV-1–infected T-cell clones selectively proliferated in the spleens of infected mice, resulting in an ATL-like leukemic phenotype.[33,41]

Presence of identical infected clones in $CD25^-$ and $CD25^+$ CD4 T-cell populations

Splenocytes from infected mice were sorted into $CD25^-$ or $CD25^+$ CD4 T cells and CD8 T cells; the PVL of each population was also determined. Most of the $CD25^+$ CD4 T cells isolated from the spleens of infected mice were provirus-positive, as was a significant proportion of $CD25^-$ CD4 T cells, whereas infection of CD8 T cells was rare (Figure 5B). Interestingly, *tax* expression in HTLV-1–infected $CD25^+$ CD4 T cells was suppressed compared with that in

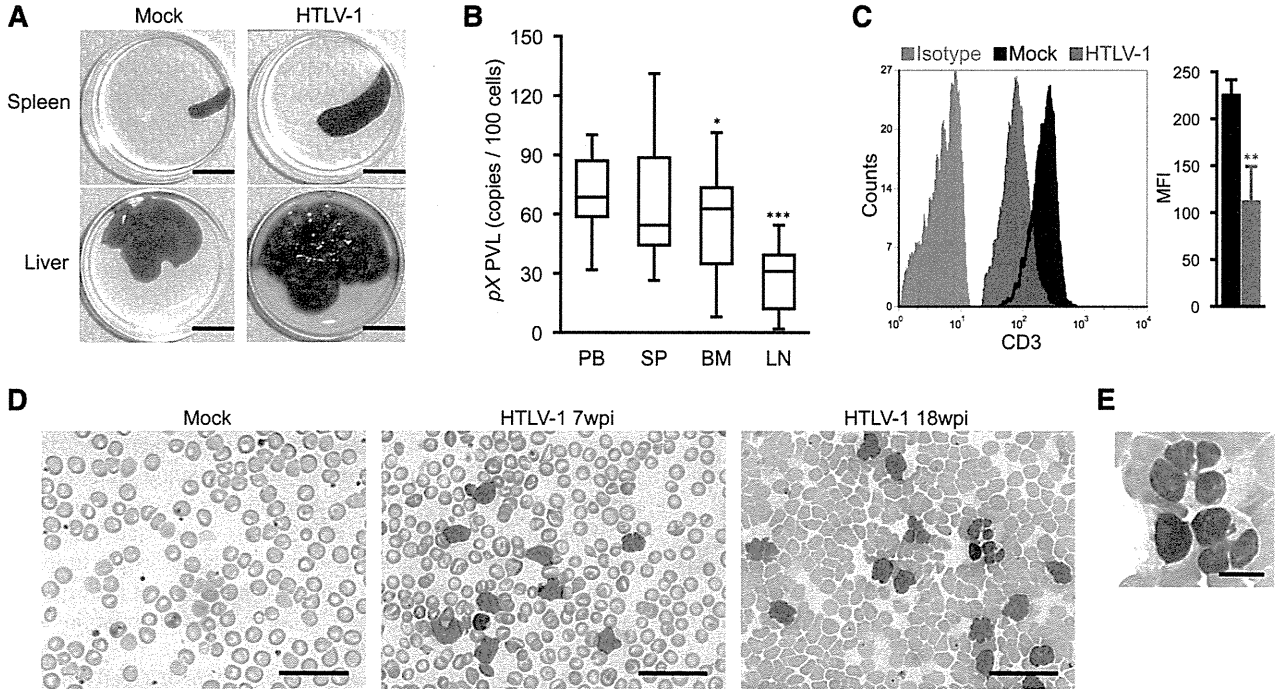

Figure 3. Splenomegaly and leukemic T-cell overgrowth in infected IBMI-huNOG mice. (A) Hepatosplenomegaly in HTLV-1–infected mice. Representative spleens and livers from mock- and HTLV-1–infected mice are shown. Scale bars in panel A represent 10 mm. (B) PVL in lymphoid organs of HTLV-1–infected mice. PVL in the peripheral blood (PB), spleen (SP), bone marrow (BM), and lymph nodes (LM) of HTLV-1–infected mice (n = 17) are shown. Box plots represent medians ± 1.5 IQR. Asterisks indicate statistical significance vs the value obtained from peripheral blood (*$P < .05$, ***$P < .001$ by paired *t* test). (C) Downregulation of CD3 on the T-cell surface. PBMCs from mock- (n = 3) and HTLV-1–infected mice (n = 18) were stained for human CD3 and analyzed by FACS. Results are presented as mean MFI ± SD of CD3 expression. (D-E) Smears of peripheral blood from HTLV-1–infected mice showing a number of leukemic cells with atypically shaped nuclei. Results from two infected mice (7 and 18 wpi, respectively) and a mock-infected mouse (at 8 mpt) are shown. Higher-magnification view of flower cells in panel D is shown in panel E. Scale bars in panels D-E represent 50 and 10 μm, respectively. Asterisks in panels B and C represent significant differences vs mock-infected mice (**$P < .01$ by Mann-Whitney *U* test).

$CD25^-$ CD4 T cells; however, higher *HBZ* expression was observed in $CD25^+$ CD4 T cells (Figure 5C).

Further clonality analysis for HTLV-1–infected $CD25^-$ and $CD25^+$ CD4 T cells isolated from the same spleen with the purity of >95% (supplemental Figure 3) revealed that the most abundant clone was the same in both T-cell populations; however, the occupancy was higher in the $CD25^+$ population (Figure 5D), indicating the preferential growth of infected clones with CD25 expression.

Induction of HTLV-1–specific adaptive immune responses in HTLV-1–infected IBMI-huNOG mice

HLA-A*24:02–restricted Tax-specific CTLs were frequently detected in ATL patients, and are known to play an important role in the control of HTLV-1–infected cells in vivo.[42-44] To investigate whether Tax-specific CTLs were induced in HTLV-1–infected mice, the IBMI-huNOG mice were generated using hematopoietic stem cells purified from the cord blood of an HLA-A*24:02 haplotype individual. HLA-A*24:02 tetramers coupled with Tax301-309 were used to detect CTLs. The cord blood HLA-A alleles used in this study are shown in supplemental Table 1. As shown in Figure 6A, Tax301-309–specific CTLs were detected in HTLV-1–infected mice at a frequency similar to that of ATL patients (0.7% ± 0.8%, n = 18),[45] whereas control tetramer CTLs specific for HIV env produced only marginal staining of CD8 T cells.

To evaluate whether functionally reactive Tax301-309–specific CTLs were present in infected mice, we cultured splenocytes from HTLV-1–infected mice in the presence of Tax peptide. Tax301-309 specific CTLs clearly proliferated following peptide stimulation; no reaction was seen in controls. Furthermore, the frequency of Tax301-309–specific CTLs in in vivo CD8 T cells was inversely correlated with the PVLs of HTLV-1–infected mice (Figure 6B). These results suggest that HTLV-1–infected mice induce functional T-cell–mediated cellular immunity against HTLV-1, which may be involved in the control of HTLV-1–infected cells in vivo.

Antibodies against HTLV-1 antigens were also detected in the plasma of infected mice as early as 2 wpi, whereas the specific antibody was not detected before infection (Figure 6C). The titer of HTLV-1–specific antibodies increased in all cases until 4 wpi, followed by a gradual decline in 67% of infected mice (4 of 6), coincident with a decrease in body weight. However, 2 of the infected mice exhibited a reactivation of antibody production at 8 wpi, suggestive of immunoglobulin class switching from IgM to IgG. In fact, HTLV-1–specific antibody titers were significantly decreased following selective depletion of human IgG, indicating the presence of functional IgG in the plasma of HTLV-1–infected mice (Figure 6D). These data clearly support the notion that the functional interaction between human T and B cells required for class switching exists in this model. Taken together, these results demonstrate that human-like adaptive immunity against HTLV-1 was established in the HTLV-1–infected IBMI-huNOG mice.

Discussion

In this study, we established a novel humanized mouse model of HTLV-1 infection. To generate humanized mice, we transplanted

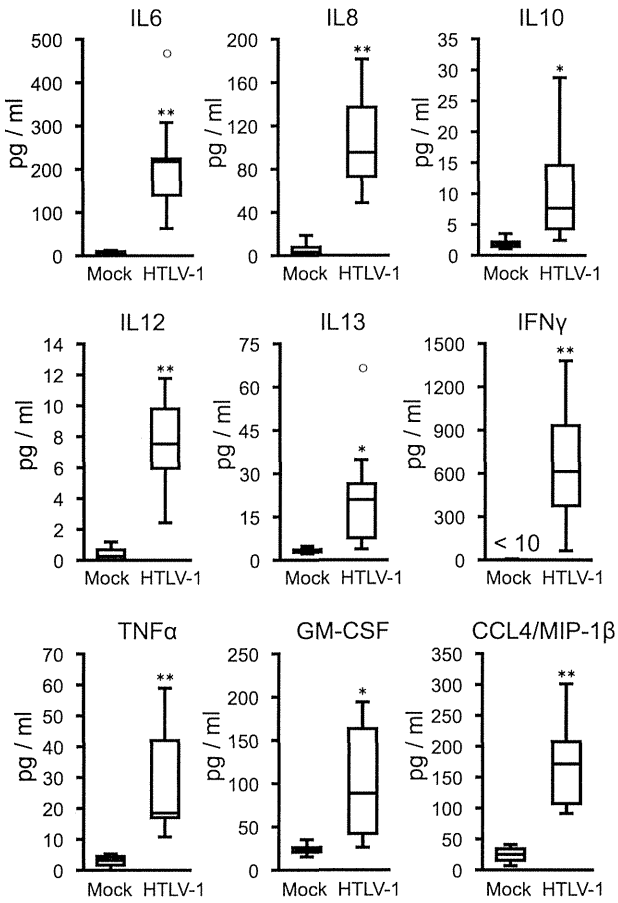

Figure 4. Induction of inflammatory cytokines in infected IBMI-huNOG mice. Human cytokine concentrations in plasma. Plasma was collected following sacrifice of mock-infected (n = 4) and HTLV-1–infected mice (n = 8). Seventeen cytokines were quantified using a cytokine bead array system. The concentrations of human IL-6, IL-8, IL-10, IL-12, IL-13, IFNγ, TNF-α, GM-CSF, and CCL4/MIP-1β are shown, all of which were significantly increased in the plasma of HTLV-1–infected mice. Increased expressions of the other 6 cytokines (IL-2, IL-4, IL-7, IL-17, G-CSF, and MCP-1) were also observed in infected mice but not statistically significant. On the other hand, little decrease in the concentrations of IL-1 and IL-5 was seen. Asterisks in each panel represent significant differences vs mock-infected mice (*$P < .05$, **$P < .01$ by Mann-Whitney *U* test).

human stem cells directly into the bone marrow cavity of NOD/Shi-SCID/IL-2Rγc null (NOG) mice using an IBMI method.

The efficacy of humanization achieved in this model is markedly superior to other procedures, such as intrahepatic or intravenous injection of human hematopoietic stem cells.[21,22,29] While T-lineage–cell populations become dominant over B-cell populations in the lymphoid organs of other humanized mouse systems within a few months after transplantation, in IBMI-huNOG mice the B-to-T-cell ratio remained constant for >8 months posttransplantation (Figure 1E). One possible explanation for this difference is that direct injection of hematopoietic stem cell preparations into the bone marrow of recipient mice improves the colonization efficiency of long-term stem cells.[27,46] Moreover, we used $CD133^+$ cells to generate IBMI-huNOG mice. CD133, the early hematopoietic progenitor cell marker, is thought to be ancestral to CD34 in human hematopoiesis.[47] Previous studies have revealed that $CD133^+$ cells were capable of differentiating not only into hematopoietic cells but also into endothelial, stromal, neuronal, and other type of cells.[47-49] It is possible that human mesenchymal stromal cells derived from $CD133^+$ cells support the development and maintenance of human B cells in the bone marrow microenvironment.

Having established a new humanized mouse model, we then infected IBMI-huNOG mice with HTLV-1 through inoculation with sublethally irradiated HTLV-1–producing cells.[28] HTLV-1–infected IBMI-huNOG mice recapitulated a large number of pathological features characteristic of ATL patients, including hyperproliferation of $CD3^+$ T cells, clonal proliferation of $CD25^+$ CD4 T cells, the appearance of flower cells in the periphery, hepatosplenomegaly, inflammatory hypercytokinemia, and down-regulation of CD3 on T cells.

Overgrowth of infected T cells was correlated with the expression of CD25 on CD4 T cells, consistent with recent reports.[17] However, the substantial proportion of $CD25^-$ CD4 T cells were also infected and identical T-cell clones, as determined by provirus integration site, were detected as the most abundant clones in both $CD25^-$ and $CD25^+$ CD4 T-cell populations, suggesting that CD25 expression likely occurs after infection in the course of clonal expansion. In addition, the expressions of *tax* and CD25 were inversely correlated. Further research will be necessary to identify molecular events associated with the suppression of *tax* expression in HTLV-1–infected $CD25^+$ CD4 T cells in relation to the development of ATL.

Banerjee et al[16] described the development of T-cell lymphoma following bone marrow transplantation of HTLV-1–infected $CD34^+/CD38^-$ hematopoietic stem cells into a NOD/SCID mouse. The lymphoma cells in these mice were capable of infiltrating into multiple organs but represented only $CD25^-$ or $CD25^{low}$ phenotypes. In contrast, HTLV-1–infected IBMI-huNOG mice developed leukemia in $CD25^+$ CD4 T cells, similar to that observed in ATL patients. The mechanism underlying this difference is unknown but may be due to differences in the developmental stage of T cells at the time of infection. Indeed, HTLV-1 infection in a different humanized mouse model, generated by intrahepatic transplantation of human $CD34^+$ stem cells into $Rag2^{-/-}\gamma c^{-/-}$ mice, induced formation of thymomas/lymphomas in mature CD4 T cells.[17] In this case, HTLV-1 infection was carried out 4 and 8 weeks after transplantation of $CD34^+$ hematopoietic stem cells, giving the human immune system time to develop. Thus the infection of $CD34^+$ stem cells per se does not appear to be sufficient for the induction of mature $CD25^+$ T cell malignancies and may require more developed lymphoid cells or a more appropriate microenvironment capable of supporting cell development.

Furthermore, HTLV-1–infected IBMI-huNOG mice almost exclusively developed leukemia, whereas HTLV-1 infection in the other humanized mouse models described above preferentially induced formation of lymphoma or thymoma. The reason for this difference is not clear but may stem from differences in the timing of T-cell infection. IBMI-huNOG mice were infected after the human hematopoietic system had been fully established, while in the other systems the infection was carried out before or shortly after stem cell transplantation.

In addition to leukemic growth of $CD25^+$ T cells, we also observed formation of flower cells in the peripheral blood of infected mice at later time points postinfection (>16 wpi). Although transformed T cells derived from Tax-transgenic mice were found to exhibit similar morphology,[15] none of the animal models described so far had recapitulated this pathology. Clonal analysis performed as part of this study demonstrated that the expansion of $CD25^+$ T-cell clones preceded the appearance of flower cells in periphery, suggesting a sequence of events that occurs during development of the malignancy. Thus, chronological

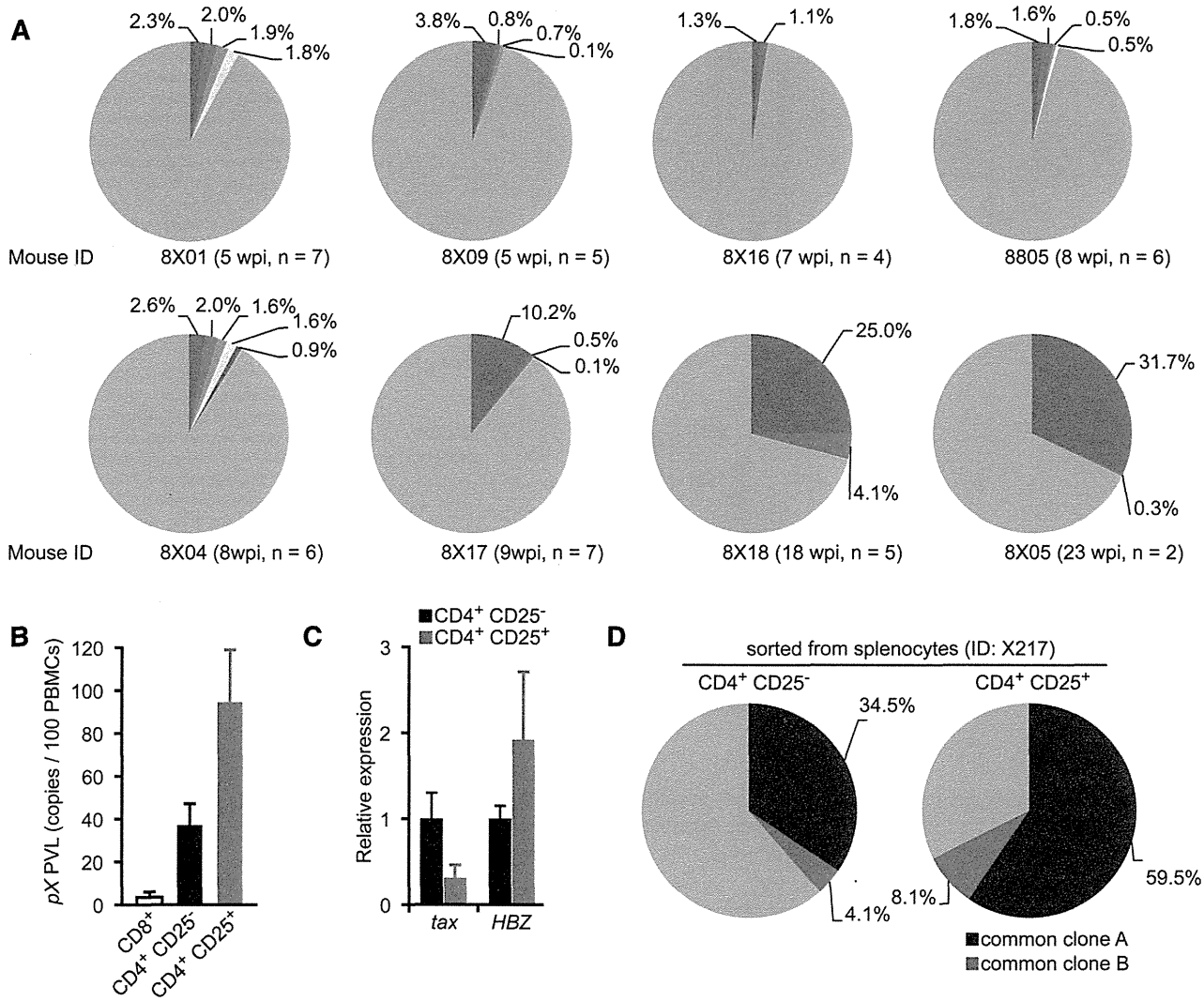

Figure 5. Progression of clonality in splenocytes of infected IBMI-huNOG. (A) Occupancy of HTLV-1–infected clones in the spleen. Abundant integration sites of HTLV-1 provirus were amplified by IL-PCR and subcloned into plasmids. The number of integration sites in each splenic DNA sample was determined by quantitative PCR using the clone-specific nucleotide sequence for each integration site. Results from 8 individual HTLV-1–infected mice are shown as pie charts. Size of the slice is proportional to the relative abundance of T-cell clones successfully amplified by IL-PCR, while data of minor clones with less than 0.1% occupancy were omitted. Gray regions represent clones with undefined integration sites. n, number of integration sites determined by nucleotide sequence of cloned PCR fragments in each mouse. (B) PVLs of specifiedT-cell populations. Splenocytes from HTLV-1–infected mice (n = 5) were sorted into $CD25^-$ or $CD25^+$ CD4 T cells and $CD8^+$ T cells. Genomic DNA isolated from each T-cell population was analyzed for PVL by real-time PCR using primers for the *pX* region of HTLV-1. (C) Comparative analysis of viral transcripts in $CD25^-$ and $CD25^+$ CD4 T-cell populations. Splenocytes from HTLV-1–infected mice (n = 5) are identical to those in mentioned above. The expression levels of *tax* (left) and *HBZ* (right) were analyzed by quantitative RT-PCR and were normalized to that of *HPRT1*. Results are presented as the fold change compared with the value in $CD25^-$ CD4 T cells. (D) Detection of common T-cell clones in the $CD25^-$ and $CD25^+$ CD4 T-cell populations. Clonal occupancy in both $CD25^-$ and $CD25^+$ populations are presented as pie charts. Two abundant common clones were analyzed for occupancy. Identified integration sites are listed in supplemental Table 5. The purity of each sorted population was >95% (supplemental Figure 3).

analysis of genetic and/or biochemical events in infected T cells from this mouse model should provide substantial information regarding the development of ATL.

We detected HLA-restricted CTLs against Tax protein of HTLV-1, as demonstrated in the peripheral blood of HTLV-1–infected carriers,[43] confirming the presence of an acquired immune response. Furthermore, the frequency of CTLs in CD8 T-cell populations were inversely correlated with the number of infected T cells in the spleen of humanized mice, similar to observations in HTLV-1–infected individuals.[43] The presence of functional T cells was also supported by the production of IgG antibodies specific to HTLV-1. Although humanized mice established by the transplantation of $CD34^+$ hematopoietic stem cells have been reported to produce antibodies against specific pathogens such as EBV,[22] HIV-1,[21] and DENV,[50] class switching from IgM to IgG was observed in only a few cases, likely due to immature T-cell development. In the IBMI-huNOG system, however, IgG production against HTLV-1 structural protein was observed after biphasic induction of antibodies after 8 weeks, indicating a functional interaction between CD4 T cells and B cells specific for viral antigens. Taken together, these data demonstrate induction of an adaptive immune response against HTLV-1 in HTLV-1–infected IBMI-huNOG mice, which may play an important role as selective pressure in the expansion of malignant T-cell clones.

In conclusion, our study demonstrates that the HTLV-1–infected IBMI-huNOG mouse represents a novel model that will facilitate elucidation of the molecular mechanism of in vivo development of ATL. Moreover, our model can also be used to develop and evaluate

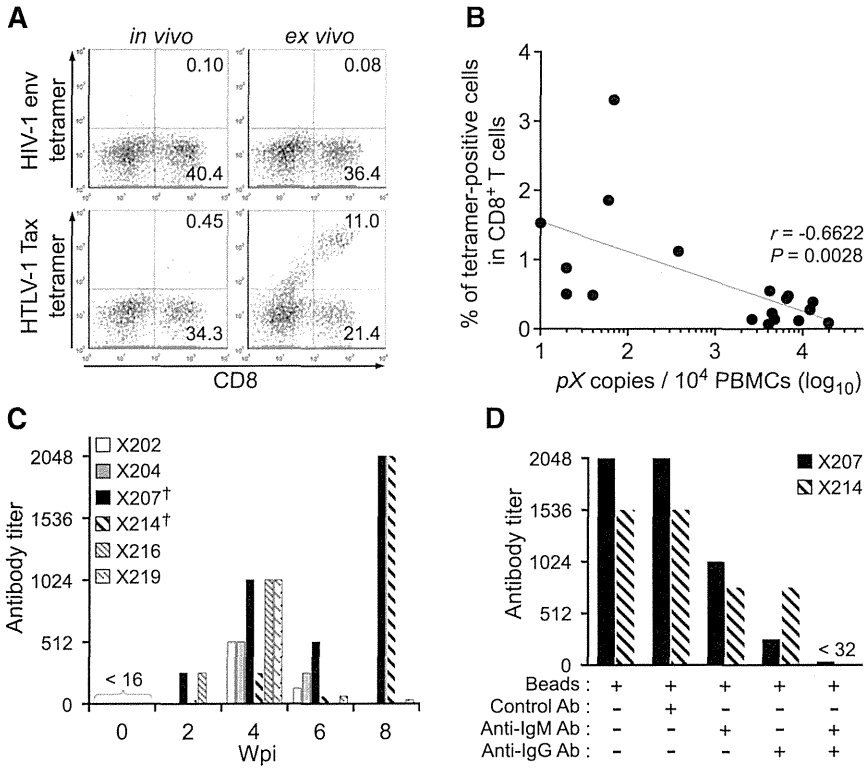

Figure 6. Induction of cellular and humoral immune responses against HTLV-1 in infected IBMI-huNOG mice. (A) Detection of HTLV-1–specific HLA-A*24:02-restricted CTLs. Splenocytes from HTLV-1–infected mice at 8 wpi were stained with human CD8 and Tax301-309 tetramer or HIV-1 env gp160 tetramer as a negative control, respectively. Representative results of tetramer-positive CD8 T cells in vivo (left) and ex vivo culture with Tax peptide (right) are shown. (B) Inverse correlation between PVL and the frequency of Tax301-309–specific CTLs. The percentages of tetramer-positive CD8 T cells and PVL in the spleens of 18 HTLV-1–infected mice are shown. One dot represents the result of an individual HTLV-1–infected mouse. Spearman's rank-correlation coefficient (r^2) was used to identify statistically significant correlations. (C) HTLV-1–specific antibody responses in HTLV-1–infected mice. HTLV-1–specific antibody titers in plasma were monitored by the particle agglutination method. Each bar represents an individual mouse. The plasma of indicated mice prior to infection were used as negative-controls (shown as 0 wpi), and these titers were undetectable level (<16). Mice with daggers (mouse ID: X207 and X214) showed biphasic induction of antibody responses; titers peaked at 8 wpi. (D) Detection of HTLV-1–specific IgM or IgG antibody. Antibody depletion was performed by addition of goat antibodies against human IgG or IgM and anti-goat antibody conjugated magnetic beads to the plasma of two mice, as shown in panel C (indicated by daggers). Bars represent antibody titers in the individual X207 and X214 mice. Ab, antibody.

novel preclinical therapies that target viral gene products or cellular molecules critical for viral replication as well as evaluate the efficacy of vaccine candidates to prevent viral expansion in vivo.

Acknowledgments

The authors thank Drs R. Tatsumi and Y. Adachi for advice in establishing humanized mice and assistance with the pathological analysis, respectively. The authors are grateful to the Japanese Red Cross Kinki Cord Blood Bank for providing the samples used in this study.

This work was supported by Grants-in-Aid for Scientific Research C from the Ministry of Education, Culture, Sports, Science and Technology of Japan (grants 21590515 and 24590562) (J.F.); a MEXT-Supported Program for the Strategic Research Foundation at Private Universities; and Health and Labour Sciences Research Grants for Research on Emerging and Re-emerging Infectious Diseases from Ministry of Health, Labour and Welfare (grant 24171601) (T.U.) (grant 23211801) (M. Tanaka).

Authorship

Contribution: K.T. and J.F. designed the research; K.T. and R.X. established and maintained humanized mice; K.T., R.X., M. Tei and T.U. carried out experiments; M. Tanaka was involved in the IL-PCR analysis; K.T., R.X., M. Tei, and J.F. analyzed results; N.T. performed statistical analysis; K.T. designed the figures; and K.T. and J.F. wrote the paper.

Conflict-of-interest disclosure: The authors declare no competing financial interests.

Correspondence: Jun-ichi Fujisawa, Department of Microbiology, Kansai Medical University, 2-5-1 Shin-machi, Hirakata, Osaka 573-1010, Japan; e-mail: fujisawa@hirakata.kmu.ac.jp.

References

1. Hinuma Y, Nagata K, Hanaoka M, et al. Adult T-cell leukemia: antigen in an ATL cell line and detection of antibodies to the antigen in human sera. *Proc Natl Acad Sci USA*. 1981;78(10):6476-6480.
2. Poiesz BJ, Ruscetti FW, Gazdar AF, Bunn PA, Minna JD, Gallo RC. Detection and isolation of type C retrovirus particles from fresh and cultured lymphocytes of a patient with cutaneous T-cell lymphoma. *Proc Natl Acad Sci USA*. 1980;77(12):7415-7419.
3. Osame M, Usuku K, Izumo S, et al. HTLV-I associated myelopathy, a new clinical entity. *Lancet*. 1986;1(8488):1031-1032.
4. Kondo T, Kono H, Miyamoto N, et al. Age- and sex-specific cumulative rate and risk of ATLL for HTLV-I carriers. *Int J Cancer*. 1989;43(6):1061-1064.
5. Boxus M, Twizere JC, Legros S, Dewulf JF, Kettmann R, Willems L. The HTLV-1 Tax interactome. *Retrovirology*. 2008;5:76.
6. Matsuoka M, Jeang KT. Human T-cell leukemia virus type 1 (HTLV-1) and leukemic transformation: viral infectivity, Tax, HBZ and therapy. *Oncogene*. 2011;30(12):1379-1389.
7. Yoshida M, Seiki M, Yamaguchi K, Takatsuki K. Monoclonal integration of human T-cell leukemia provirus in all primary tumors of adult T-cell leukemia suggests causative role of human T-cell leukemia virus in the disease. *Proc Natl Acad Sci USA*. 1984;81(8):2534-2537.
8. Shimoyama M, Minato K, Tobinai K, et al. Atypical adult T-cell leukemia-lymphoma: diverse clinical manifestations of adult T-cell leukemia-lymphoma. *Jpn J Clin Oncol*. 1983;13(Suppl 2):165-187.
9. Okayama A, Tachibana N, Ishihara S, et al. Increased expression of interleukin-2 receptor alpha on peripheral blood mononuclear cells in HTLV-I tax/rex mRNA-positive asymptomatic carriers. *J Acquir Immune Defic Syndr Hum Retrovirol*. 1997;15(1):70-75.

10. Bieberich CJ, King CM, Tinkle BT, Jay G. A transgenic model of transactivation by the Tax protein of HTLV-I. *Virology.* 1993;196(1):309-318.
11. Feuer G, Zack JA, Harrington WJ Jr, et al. Establishment of human T-cell leukemia virus type I T-cell lymphomas in severe combined immunodeficient mice. *Blood.* 1993;82(3): 722-731.
12. Kondo A, Imada K, Hattori T, et al. A model of in vivo cell proliferation of adult T-cell leukemia. *Blood.* 1993;82(8):2501-2509.
13. Furuta RA, Sugiura K, Kawakita S, Inada T, Ikehara S, Matsuda T, Fujisawa J. Mouse model for the equilibration interaction between the host immune system and human T-cell leukemia virus type 1 gene expression. *J Virol.* 2002;76(6): 2703-2713.
14. Dewan MZ, Terashima K, Taruishi M, et al. Rapid tumor formation of human T-cell leukemia virus type 1-infected cell lines in novel NOD-SCID/ gammac(null) mice: suppression by an inhibitor against NF-kappaB. *J Virol.* 2003;77(9): 5286-5294.
15. Hasegawa H, Sawa H, Lewis MJ, et al. Thymus-derived leukemia-lymphoma in mice transgenic for the Tax gene of human T-lymphotropic virus type I. *Nat Med.* 2006;12(4):466-472.
16. Banerjee P, Tripp A, Lairmore MD, et al. Adult T-cell leukemia/lymphoma development in HTLV-1-infected humanized SCID mice. *Blood.* 2010;115(13):2640-2648.
17. Villaudy J, Wencker M, Gadot N, et al. HTLV-1 propels thymic human T cell development in "human immune system" $Rag2^{-/-}$ gamma $c^{-/-}$ mice. *PLoS Pathog.* 2011;7(9):e1002231.
18. Satou Y, Yasunaga J, Zhao T, et al. HTLV-1 bZIP factor induces T-cell lymphoma and systemic inflammation in vivo. *PLoS Pathog.* 2011;7(2): e1001274.
19. Kazanji M. HTLV type 1 infection in squirrel monkeys (Saimiri sciureus): a promising animal model for HTLV type 1 human infection. *AIDS Res Hum Retroviruses.* 2000;16(16):1741-1746.
20. Lairmore MD, Silverman L, Ratner L. Animal models for human T-lymphotropic virus type 1 (HTLV-1) infection and transformation. *Oncogene.* 2005;24(39):6005-6015.
21. Watanabe S, Terashima K, Ohta S, et al. Hematopoietic stem cell-engrafted NOD/SCID/ IL2Rgamma null mice develop human lymphoid systems and induce long-lasting HIV-1 infection with specific humoral immune responses. *Blood.* 2007;109(1):212-218.
22. Yajima M, Imadome K, Nakagawa A, et al. A new humanized mouse model of Epstein-Barr virus infection that reproduces persistent infection, lymphoproliferative disorder, and cell-mediated and humoral immune responses. *J Infect Dis.* 2008;198(5):673-682.
23. Hasegawa A, Ohashi T, Hanabuchi S, Kato H, Takemura F, Masuda T, Kannagi M. Expansion of human T-cell leukemia virus type 1 (HTLV-1) reservoir in orally infected rats: inverse correlation with HTLV-1-specific cellular immune response. *J Virol.* 2003;77(5):2956-2963.
24. Kannagi M, Hasegawa A, Kinpara S, Shimizu Y, Takamori A, Utsunomiya A. Double control systems for human T-cell leukemia virus type 1 by innate and acquired immunity. *Cancer Sci.* 2011; 102(4):670-676.
25. Ito M, Hiramatsu H, Kobayashi K, et al. NOD/SCID/gamma(c)(null) mouse: an excellent recipient mouse model for engraftment of human cells. *Blood.* 2002;100(9):3175-3182.
26. Kushida T, Inaba M, Hisha H, et al. Intra-bone marrow injection of allogeneic bone marrow cells: a powerful new strategy for treatment of intractable autoimmune diseases in MRL/lpr mice. *Blood.* 2001;97(10):3292-3299.
27. Wang J, Kimura T, Asada R, et al. SCID-repopulating cell activity of human cord blood-derived CD34- cells assured by intra-bone marrow injection. *Blood.* 2003;101(8):2924-2931.
28. Miyoshi I, Kubonishi I, Yoshimoto S, et al. Type C virus particles in a cord T-cell line derived by co-cultivating normal human cord leukocytes and human leukaemic T cells. *Nature.* 1981; 294(5843):770-771.
29. Nie C, Sato K, Misawa N, et al. Selective infection of CD4+ effector memory T lymphocytes leads to preferential depletion of memory T lymphocytes in R5 HIV-1-infected humanized NOD/SCID/IL-2Rgammanull mice. *Virology.* 2009;394(1):64-72.
30. Takamori A, Hasegawa A, Utsunomiya A, et al. Functional impairment of Tax-specific but not cytomegalovirus-specific CD8+ T lymphocytes in a minor population of asymptomatic human T-cell leukemia virus type 1-carriers. *Retrovirology.* 2011;8:100.
31. Ueno S, Umeki K, Takajo I, et al. Proviral loads of human T-lymphotropic virus Type 1 in asymptomatic carriers with different infection routes. *Int J Cancer.* 2012;130(10):2318-2326.
32. Etoh K, Tamiya S, Yamaguchi K, et al. Persistent clonal proliferation of human T-lymphotropic virus type I-infected cells in vivo. *Cancer Res.* 1997; 57(21):4862-4867.
33. Umeki K, Hisada M, Maloney EM, Hanchard B, Okayama A. Proviral loads and clonal expansion of HTLV-1-infected cells following vertical transmission: a 10-year follow-up of children in Jamaica. *Intervirology.* 2009;52(3):115-122.
34. Hiramatsu H, Nishikomori R, Heike T, Ito M, Kobayashi K, Katamura K, Nakahata T. Complete reconstitution of human lymphocytes from cord blood CD34+ cells using the NOD/SCID/ gammacnull mice model. *Blood.* 2003;102(3): 873-880.
35. Nitta T, Tanaka M, Sun B, Hanai S, Miwa M. The genetic background as a determinant of human T-cell leukemia virus type 1 proviral load. *Biochem Biophys Res Commun.* 2003;309(1):161-165.
36. Yamano Y, Araya N, Sato T, et al. Abnormally high levels of virus-infected IFN-gamma+ CCR4+ CD4+ CD25+ T cells in a retrovirus-associated neuroinflammatory disorder. *PLoS ONE.* 2009;4(8):e6517.
37. Matsuda M, Maeda Y, Shirakawa C, et al. CD3 down-regulating factor in sera and culture supernatants of leukaemic cells from patients with adult T cell leukaemia. *Br J Haematol.* 1993;83(2): 212-217.
38. Yamada Y, Ohmoto Y, Hata T, et al. Features of the cytokines secreted by adult T cell leukemia (ATL) cells. *Leuk Lymphoma.* 1996;21(5-6): 443-447.
39. Chiba K, Hashino S, Izumiyama K, Toyoshima N, Suzuki S, Kurosawa M, Asaka M. Multiple osteolytic bone lesions with high serum levels of interleukin-6 and CCL chemokines in a patient with adult T cell leukemia. *Int J Lab Hematol.* 2009;31(3):368-371.
40. Chen J, Petrus M, Bryant BR, et al. Autocrine/ paracrine cytokine stimulation of leukemic cell proliferation in smoldering and chronic adult T-cell leukemia. *Blood.* 2010;116(26):5948-5956.
41. Ohshima K, Mukai Y, Shiraki H, Suzumiya J, Tashiro K, Kikuchi M. Clonal integration and expression of human T-cell lymphotropic virus type I in carriers detected by polymerase chain reaction and inverse PCR. *Am J Hematol.* 1997; 54(4):306-312.
42. Kurihara K, Harashima N, Hanabuchi S, et al. Potential immunogenicity of adult T cell leukemia cells in vivo. *Int J Cancer.* 2005;114(2):257-267.
43. Akimoto M, Kozako T, Sawada T, et al. Anti-HTLV-1 tax antibody and tax-specific cytotoxic T lymphocyte are associated with a reduction in HTLV-1 proviral load in asymptomatic carriers. *J Med Virol.* 2007;79(7):977-986.
44. Harashima N, Kurihara K, Utsunomiya A, et al. Graft-versus-Tax response in adult T-cell leukemia patients after hematopoietic stem cell transplantation. *Cancer Res.* 2004;64(1):391-399.
45. Kozako T, Arima N, Toji S, et al. Reduced frequency, diversity, and function of human T cell leukemia virus type 1-specific CD8+ T cell in adult T cell leukemia patients. *J Immunol.* 2006; 177(8):5718-5726.
46. Nakamura K, Inaba M, Sugiura K, Yoshimura T, Kwon AH, Kamiyama Y, Ikehara S. Enhancement of allogeneic hematopoietic stem cell engraftment and prevention of GVHD by intra-bone marrow bone marrow transplantation plus donor lymphocyte infusion. *Stem Cells.* 2004; 22(2):125-134.
47. Jaatinen T, Hemmoranta H, Hautaniemi S, et al. Global gene expression profile of human cord blood-derived CD133+ cells. *Stem Cells.* 2006; 24(3):631-641.
48. Herrera MB, Bruno S, Buttiglieri S, et al. Isolation and characterization of a stem cell population from adult human liver. *Stem Cells.* 2006;24(12): 2840-2850.
49. Martin-Rendon E, Hale SJ, Ryan D, et al. Transcriptional profiling of human cord blood CD133+ and cultured bone marrow mesenchymal stem cells in response to hypoxia. *Stem Cells.* 2007;25(4):1003-1012.
50. Kuruvilla JG, Troyer RM, Devi S, Akkina R. Dengue virus infection and immune response in humanized $RAG2(^{-/-})gamma(c)(^{-/-})$ (RAG-hu) mice. *Virology.* 2007;369(1):143-152.

INTERNAL MEDICINE

□ ORIGINAL ARTICLE □

Cerebrospinal Fluid Neopterin, but not Osteopontin, is a Valuable Biomarker for the Treatment Response in Patients with HTLV-I-associated Myelopathy

Masahiro Nagai, Tomoaki Tsujii, Hirotaka Iwaki, Noriko Nishikawa and Masahiro Nomoto

Abstract

Objective The concentrations of neopterin and osteopontin in the cerebrospinal fluid (CSF) were measured in patients with HTLV-I-associated myelopathy/tropical spastic paraparesis (HAM/TSP) in order to evaluate their utility as biomarkers for the treatment response.

Methods Seven HAM/TSP patients were treated intravenously with high-dose methylprednisolone (1,000 mg/day) for 3 days. CSF samples were collected before and after the treatment. The neopterin and osteopontin concentrations were determined using high-performance liquid chromatography (HPLC) and an enzyme immunoassay, respectively. The clinical symptoms were evaluated using the Osame Motor Disability Score and the Urinary Disturbance Score.

Results Four out of the seven patients showed an improvement in motor function with the treatment, and were therefore classed as responders. The pre-treatment CSF neopterin concentration exceeded the upper limit of normal in all seven of the patients, and tended to be higher in treatment responders as compared to non-responders. The CSF neopterin concentration was reduced following treatment in all patients. The mean CSF neopterin concentration significantly ($p<0.01$) decreased following treatment by almost 60% (from 124.1±79.9 nmol/L to 49.2±29.8 nmol/L). The mean CSF osteopontin concentration was significantly ($p<0.01$) higher in the HAM/TSP patients in comparison to the 18 HTLV-1-seronegative patients who were designated as controls (9.54±4.53 mg/L vs. 3.72±3.04 mg/L). No significant ($p=0.47$) reduction of the CSF osteopontin concentration was observed following the intravenous administration of high-dose methylprednisolone.

Conclusion These results indicate that the CSF neopterin concentration, but not the osteopontin concentration, is a potentially valuable biomarker for monitoring the treatment response in HAM/TSP patients. Furthermore, high pre-treatment CSF neopterin concentrations may be a predictive biomarker for a response to intravenous high-dose methylprednisolone therapy.

Key words: HTLV-I, HAM/TSP, cerebrospinal fluid, neopterin, osteopontin, methylprednisolone

(Intern Med 52: 2203-2208, 2013)
(DOI: 10.2169/internalmedicine.52.0869)

Introduction

Human T-cell lymphotropic virus type I (HTLV-I) is an exogenous human retrovirus that has been demonstrated to be the etiological agent in adult T-cell leukemia as well as in a progressive neurological disease called HTLV-I-associated myelopathy/tropical spastic paraparesis (HAM/TSP). The vast majority of HTLV-I-infected individuals are clinically asymptomatic, with <5% of infected individuals ever developing HAM/TSP. Clinically, HAM/TSP is characterized by muscle weakness, hyperreflexia, spasticity in the lower extremities and urinary disturbance associated with the preferential damage of the thoracic spinal cord (1). Although it is not yet completely understood how HTLV-I causes HAM/TSP, it is believed that increased HTLV-I

Department of Neurology and Clinical Pharmacology, Ehime University Graduate School of Medicine, Japan
Received for publication April 26, 2013; Accepted for publication June 2, 2013
Correspondence to Dr. Masahiro Nomoto, nomoto@m.ehime-u.ac.jp

Table 1. **Patient Characteristics**

Patient no.	Age (years)	Sex	Disease duration (years)	CSF anti-HTLV-I antibody titer
1	70	M	13	1:512
2	81	F	2	1:800
3	48	F	2	1:256
4	48	F	4	1:800
5	77	F	5	1:512
6	60	F	2	1:512
7	56	F	10	1:128

F: female, M: male

Table 2. **Rating Scale for the Osame Motor Disability Score**

0	Normal walking and running
1	Normal gait but runs slowly
2	Abnormal gait
3	Abnormal gait and unable to run
4	Needs support while using stairs
5	Needs 1-hand support in walking
6	Needs 2-hand support in walking
7	Needs 2-hand support in walking and is limited to 10 m
8	Needs 2-hand support in walking and is limited to 5 m
9	Unable to walk but able to crawl on hands and knees
10	Crawls with hands
11	Unable to crawl but can turn sideways in bed
12	Unable to turn sideways but can move toes
13	Completely bedridden

proviral loads and immune responses to HTLV-I infected cells play a pivotal role in the pathogenesis of this disorder (2).

Consequently, therapeutic strategies for HAM/TSP patients are directed towards these pathogenic phenomena. The first therapeutic strategy is to reduce HTLV-I loads, although anti-retroviral reagents such as reverse transcriptase inhibitors seem to be less effective for HTLV-I infections than for human immunodeficiency virus (HIV) infections. The second therapeutic strategy is to modulate the abnormal immune responses in HAM/TSP patients. Several immunosuppressive or immunomodulating therapies have been tried, including corticosteroids, interferon-α (IFN-α), azathioprine and plasmapheresis (3). Chronic oral prednisolone therapy was empirically the most effective for the improvement the neurological impairment that is associated with HAM/TSP. However, adverse events such as osteoporosis, glucose intolerance and gastroduodenal ulceration have limited its use for HAM/TSP patients, especially elderly postmenopausal women. We have chosen IV high-dose methylprednisolone as a first-line therapy because this treatment has a better tolerability profile than chronic oral prednisolone therapy. Another reason is because IV high-dose methylprednisolone therapy has been extensively and successfully used for patients with relapses of multiple sclerosis or other immune-mediated neurological disorders.

Although the anti-HTLV-I antibody titer in the cerebrospinal fluid (CSF) is used as a diagnostic biomarker of HAM/TSP, it is inadequate as a biomarker for monitoring the treatment response. However, increased CSF neopterin concentrations have been previously reported in patients with HAM/TSP (4, 5). Neopterin is a pyrazino-pyrimidine compound that is produced by macrophages after stimulation by IFN-γ from activated T cells. The concentration of neopterin in the CSF has been used as a biomarker for cellular immune response in the central nervous system (CNS). Osteopontin has multiple functions and is involved in the recruitment of macrophage and T cells in inflammatory lesions. Osteopontin enhances IFN-γ and interleukin (IL)-12 production and depresses the release of IL-10 from immune cells (6). It is up-regulated in the brains of patients with multiple sclerosis and in the spinal cords of mice with experimental autoimmune encephalomyelitis (7, 8). It is therefore believed that both neopterin and osteopontin could be valuable biomarkers for indicating the severity of inflammation and the degree of T cell activation in the CNS.

Chronic oral prednisolone therapy decreases CSF neopterin concentrations in HAM/TSP patients (3). However, it is not yet known if CSF neopterin concentrations change rapidly after treatment and might, therefore, be useful in predicting the response to corticosteroid therapy. The CSF osteopontin concentrations in HAM/TSP patients have not yet been investigated. We herein present the results of our study in which we monitored the CSF neopterin and osteopontin concentrations before and after IV high-dose methylprednisolone therapy in patients with HAM/TSP in order to evaluate their utility as biomarkers for treatment response.

Materials and Methods

The diagnosis of HAM/TSP was made according to the current WHO diagnosis guidelines. The anti-HTLV-I antibody titers were measured using a particle-agglutination (PA) test. The characteristics of the seven patients with HAM/TSP who were recruited are summarized in Table 1. They had not been previously treated with either immunosuppressive or immunomodulating agents. They were treated with IV infusions of high-dose methylprednisolone (1,000 mg/day) for 3 days following their hospital admission. None of the patients received any additional oral corticosteroid therapy following the IV administration of high-dose methylprednisolone. The Osame Motor Disability Score (OMDS) and the Urinary Disturbance Score (UDS) were used for the clinical evaluation. The OMDS rating scale is shown in Table 2. The UDS was calculated from the sum of the scores (0=normal, 1=slight, 2=moderate, 3=severe) for three symptoms (increased frequency of urination, feeling of residual urine, incontinence). CSF was obtained from each patient with written informed consent. Lumbar punctures were performed before and within 7 days of treatment completion. The collected CSF was stored at -80℃ until analyzed. The study was approved by the hospital ethics committee.

The CSF neopterin concentrations were measured using high-performance liquid chromatography (HPLC) with fluorometric detection. Thawed CSF aliquots (100 μL) were acidified with ice-cold 0.1 M HCl (100 μL) and kept on ice.

A mixture of 1% I_2 and 2% KI in 0.1 M HCl (50 μL) was then added, and the samples were incubated at room temperature under dark conditions. An aqueous solution of 1.5% ascorbic acid (50 μL) was then added to the mixture, which was then centrifuged at 10,000 rpm for 1 min. The supernatant (100 μL) was injected into a C18 column (150× 2.1 mm) with 3.5% methanol in water as the mobile phase. The quantification of osteopontin in the CSF samples was performed using a commercially available enzyme immunoassay kit (human osteopontin assay kit, Immuno-Biological Laboratories, Japan) according to the manufacturer's protocol.

Statistical analysis was performed using the JMP10 software program (SAS). The results are expressed as mean±SD and median values. The paired data from before and after treatment were analyzed by Wilcoxon's signed-rank test. The Mann-Whitney U test was used to compare groups. p values of <0.05 were considered to be statistically significant.

Results

Four out of the seven patients showed improvement in their motor function after treatment with IV high-dose methylprednisolone. One patient improved by two grades and the others improved by one grade on the OMDS rating scale (Table 3). An improvement in the urinary disturbance score was observed in four patients (Table 3). Three of the patients showed improvements on both scales, while one patient showed an improvement in the urinary disturbance score without an associated improvement in motor function and a second patient showed improved motor function without an improvement in the urinary disturbance score. Five patients had sensory disturbance (pain and numbness of lower limbs and back pain) before the treatment. The treatment alleviated pain in all five patients.

The CSF neopterin concentrations exceeded the upper limit of normal (30 nmol/L) in all of the patients before treatment. The mean CSF neopterin concentration was 124.1±79.9 nmol/L (median 89.9 nmol/L) for all seven patients prior to treatment. The CSF neopterin concentrations decreased in all of the patients after IV high-dose methylprednisolone therapy. The mean CSF neopterin concentration was significantly ($p<0.01$) reduced by almost 60% after treatment to 49.2±29.8 nmol/L (median: 43.4 nmol/L) (Table 4). The changes in the CSF neopterin concentrations according to the treatment parameters for each patient are shown in Fig. 1.

Table 3. **Changes in the Disability Scores after IV High-dose Methylprednisolone Therapy**

Patient no.	OMDS		UDS	
	Before	After	Before	After
1	5	4	6	5
2	10	8	9	7
3	4	4	5	3
4	3	3	3	3
5	5	4	3	3
6	10	9	7	6
7	5	5	3	3

OMDS: Osame Motor Disability Score, UDS: Urinary Disturbance Score

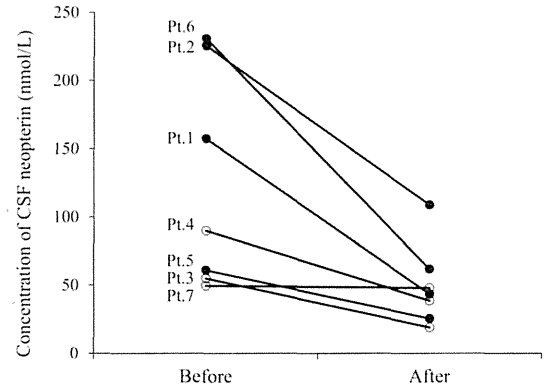

Figure 1. **The CSF neopterin concentrations before and after IV high-dose methylprednisolone therapy. The closed and open symbols indicate clinical responders and non-responders, respectively.**

Table 4. **Changes in the CSF Parameters after IV High-dose Methylprednisolone Therapy**

Patient no.	Neopterin (nmol/L)		Osteopontin (mg/L)		anti-HTLV-I antibody titer		Cells (/μL)		Protein (mg/dL)	
	Before	After	Before	After	Before	After	Before	After	Before	After
1	157.4	43.4	10.69	13.46	1:512	1:512	6	2	25	27
2	225.5	108.7	7.22	9.36	1:800	1:256	10	8	54	50
3	54.9	18.9	3.67	5.05	1:256	1:128	6	7	45	29
4	89.9	38.5	13.15	12.33	1:800	1:800	7	6	50	44
5	60.9	25.4	4.66	4.81	1:512	1:128	3	3	39	35
6	230.8	61.7	16.02	11.50	1:512	1:512	12	6	52	29
7	49.5	47.8	11.36	3.70	1:128	1:256	5	7	20	23

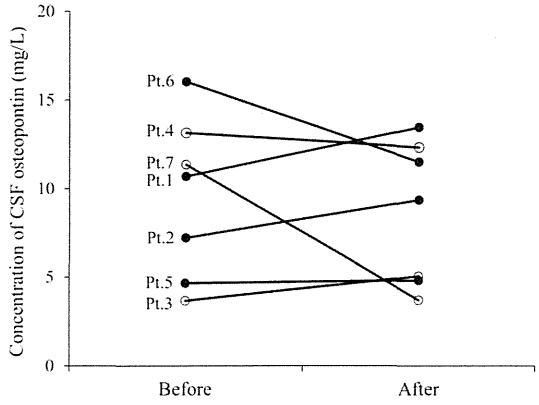

Figure 2. **The CSF osteopontin concentrations before and after IV high-dose methylprednisolone therapy. The closed and open symbols indicate clinical responders and non-responders, respectively.**

The mean CSF osteopontin concentration was 9.54±4.53 mg/L (median 10.69 mg/L) prior to treatment. Unlike for neopterin, our laboratory had not yet set an upper limit of normal for CSF osteopontin. We therefore compared CSF osteopontin concentrations for our seven HAM/TSP patients to those for 18 HTLV-I-seronegative patients with spondylosis as a control group. The mean CSF osteopontin concentration was 3.72±3.04 mg/L (median 3.52 mg/L) in the control group. The pre-treatment CSF osteopontin concentration in our seven HAM/TSP patients was significantly ($p<0.01$) higher than that of the control group. The mean CSF osteopontin concentration was 8.6±4.03 mg/L (median: 9.36 mg/L) after treatment in the seven HAM/TSP patients, which was not significantly ($p=0.47$) different than the pre-treatment values (Table 4). The pre-treatment and post-treatment CSF osteopontin concentrations for each HAM/TSP patient are shown in Fig. 2.

We defined HAM/TSP patients who showed an OMDS improvement as responders. The mean pre-treatment CSF neopterin concentration in responders (n=4) was 168.7±79.2 nmol/L (median 191.5 nmol/L), but only 64.8±22.0 nmol/L (median 54.9 nmol/L) in non-responders (n=3). While the pre-treatment CSF neopterin concentrations tended to be higher among responders compared to non-responders, the difference was not statistically significant ($p=0.056$). The mean pre-treatment CSF osteopontin concentration was 9.64±4.91 mg/L (median 8.95 mg/L) in responders and 9.34±5.04 mg/L (median 11.36 mg/L) in non-responders with no significant difference between the groups ($p=0.43$).

The HTLV-I antibody titer, and the number of cells and the amount of protein in the CSF were not significantly altered by the treatment (Table 4).

The IV high-dose methylprednisolone therapy was well tolerated by all of the patients. Although insomnia was observed as an adverse effect of treatment, it was transient. No serious adverse events were observed.

Discussion

We herein demonstrate that the CSF neopterin concentration significantly decreases following IV high-dose methylprednisolone therapy in patients with HAM/TSP. While the pre-treatment CSF osteopontin concentrations were significantly higher in HAM/TSP patients as compared to the controls, there were no statistically significant changes in the CSF osteopontin concentrations after treatment.

The coexistence of a high HTLV-I proviral load and HTLV-I-specific T cells is an important feature of HAM/TSP (9). This distinguishing feature is observed in both peripheral blood and CSF of patients with HAM/TSP (9, 10). Histopathological studies indicate the existence of HTLV-I-infected cells as well as a local inflammatory response in the spinal cord lesions of HAM/TSP patients (11, 12). It is therefore believed that the immune response to HTLV-I likely contributes to the inflammatory process of the CNS lesions in HAM/TSP patients and causes the clinical symptoms of HAM/TSP. Activated lymphocytes and macrophages up-regulate the production of pro-inflammatory cytokines such as IL-1, IL-6 and IFN-γ (13). The significant elevation of the levels of these cytokines has been described in the CSF of HAM/TSP patients (14, 15). High values of CSF neopterin have also been reported in HAM/TSP patients (4, 5). Neopterin is released by stimulated macrophages, and the concentration of CSF neopterin reflects the degree of the inflammatory response in the CNS. The concentration of CSF neopterin is significantly correlated with the HTLV-I proviral load, which is an important risk factor for the development of HAM/TSP (10). The CSF neopterin concentration is therefore useful as an adjunct to the diagnosis of HAM/TSP. In our study, we confirmed the elevation of CSF neopterin concentrations in HAM/TSP patients.

Moreover, we also demonstrated that CSF osteopontin concentrations are increased in HAM/TSP patients. To the best of our knowledge, this is the first report concerning osteopontin concentrations in HAM/TSP patients. Osteopontin is a secreted phosphoprotein that is produced by many kinds of cells including osteoblasts, activated lymphocytes, macrophages, vascular smooth muscle cells and kidney cells (16). It has a multifunctional capacity, and is involved in bone remodeling, tumor progression, atherosclerosis, inflammation and immunity (16). Osteopontin promotes the production of pro-inflammatory cytokines such as IL-12 and IFN-γ (6). Several studies have reported that osteopontin concentrations are significantly elevated in the CSF of patients with multiple sclerosis (17-19). Our finding suggests that a chronic inflammatory response in the CNS lesions of HAM/TSP is reflected by the CSF osteopontin concentrations as well as the CSF neopterin concentrations. If so, which is the better diagnostic marker for HAM/TSP? The CSF neopterin concentrations exceeded the upper limit of normal in all HAM/TSP patients. However, the CSF osteopontin concentrations in three of the seven HAM/TSP patients overlapped the range

measured for the control group. Thus, the CSF neopterin concentration would appear to be more suitable for discriminating HAM/TSP and non-HAM/TSP patients than CSF osteopontin concentration.

Various treatments have been tried for HAM/TSP patients (3). Almost all of the studies have been open-label trials or case series with the exception of a multicenter, randomized placebo-controlled, double-blind study of an IFN-α trial in Japan (20). However, no study has conclusively demonstrated a long-term clinical benefit. Well-designed clinical trials are therefore necessary in order to develop effective therapies which may improve the long-term prognoses for HAM/TSP patients (21). In addition, validated surrogate biomarkers are required for the determination of the effectiveness of investigational treatments.

It has been previously reported that approximately 70% of HAM/TSP patients who are treated with a chronic oral administration of prednisolone (n=131) improved by at least one OMDS grade (3). Furthermore, the treatment significantly decreased the reported CSF neopterin concentrations in 16 patients. The mean CSF neopterin concentration was also reduced from 155.4 nmol/L to 79.5 nmol/L by IV high-dose methylprednisolone therapy in eight of the previously reported patients, but the change was not statistically significant (3). Unfortunately, the timing of the CSF sampling after IV high-dose methylprednisolone therapy was not specified in that publication. The timing of CSF sampling is likely critical with such short-term therapies as IV high-dose methylprednisolone, since the CSF neopterin concentration seems to increase after the discontinuation of treatment. In our study, the CSF samples were collected within 7 days of the completion of the IV high-dose methylprednisolone therapy in order to attenuate the impact of the change on the CSF neopterin concentration. The CSF neopterin concentration changed rapidly after IV high-dose methylprednisolone therapy. This finding suggests that CSF neopterin is a sensitive biomarker for the evaluation of the early-phase response to treatments in HAM/TSP patients. This feature may be partially due to the short half-life of neopterin which has been estimated to be 90 minutes in the circulation (22). In contrast, there was no significant change in the CSF osteopontin concentrations that were was observed after IV high-dose methylprednisolone therapy in the HAM/TSP patients. Even though there is a possibility that a change in the CSF osteopontin concentration may arise several days after the treatment, it is clear that the CSF osteopontin concentration is unreliable as a biomarker for the assessment of an early-phase response to treatment. Although the influence of IV high-dose methylprednisolone therapy on HTLV-I proviral loads is still unclear, the therapy doesn't seem to reduce HTLV-I proviral loads. It has been reported that the osteopontin gene was transactivated by HTLV-I Tax protein (23). If the elevation of the CSF osteopontin levels in HAM/TSP patients is due to an HTLV-I infection of the osteopontin producing cells, but not the inflammatory response, then the unchanged osteopontin levels by IV high-dose methylprednisolone therapy are thus thought to be understandable.

Although it was not a statistically significant difference, and it is most likely due to the small number of patients, the pre-treatment CSF neopterin concentrations of those patients who responded to the IV high-dose methylprednisolone therapy tended to be higher than those of non-responders. This suggests that patients with relatively high values of CSF neopterin may have a more favorable response to IV high-dose methylprednisolone therapy. Additional patients need to be examined in order to confirm the belief that CSF neopterin is useful as a predictive biomarker for responders to IV high-dose methylprednisolone therapy.

The mechanism of action of for the corticosteroids on HAM/TSP remains to be elucidated. The anti-inflammatory properties of the corticosteroids may attenuate the degree of the inflammatory response in spinal cord lesions. This non-specific anti-inflammatory effect may result in clinical improvements in the patients, especially when the inflammation is very intense. Moreover, corticosteroids may also affect the HTLV-I infected cells or the immune response to HTLV-I. It has been demonstrated that betamethasone therapy decreased $CD4^+Tax^+$ T cells and increased $CD4^+Foxp3^+$ T cells (regulatory T cells) in the peripheral blood samples of patients with HAM/TSP (24). Corticosteroids therapy may reduce the erratic IFN-γ production by T-cells in patients with HAM/TSP, which is then followed by a reduction of neopterin release by the stimulated macrophages.

Our study did not address how long the clinical effect and the reduction of CSF neopterin concentration lasted after the IV high-dose methylprednisolone therapy had been discontinued. An open-label clinical trial of IV high-dose methylprednisolone has been reported from Brazil, in which 39 patients with HAM/TSP received IV high-dose methylprednisolone every 3-4 months (25). The Incapacity Status Scale showed a significant neurological improvement of 24.5% after a mean follow-up of 2.2 years. However, the CSF biomarkers were not reported in that trial. Further study will therefore be needed to clarify the long-term changes in the CSF neopterin concentration following the treatment of HAM/TSP patients.

In conclusion, our results indicate that the concentration of CSF neopterin, but not that of osteopontin, is a potentially valuable biomarker for monitoring treatment response in HAM/TSP patients. In addition, high pre-treatment CSF neopterin concentrations may be a predictive biomarker for response to IV high-dose methylprednisolone therapy.

The authors state that they have no Conflict of Interest (COI).

Acknowledgement

This study was supported by Grant-in-Aids for Orphan and Neurodegenerative Disorders from the Ministry of Health, Labour and Welfare, GJTS, and a Grant of Ehime University. The authors wish to thank Ms. Madoka Kubo for her excellent technical assistance.

References

1. Osame M, Usuku K, Izumo S, et al. HTLV-I associated myelopathy, a new clinical entity. Lancet **1**: 1031-1032, 1986.
2. Nagai M, Osame M. Human T-cell lymphotropic virus type I and neurological diseases. J Neurovirol **9**: 228-235, 2003.
3. Nakagawa M, Nakahara K, Maruyama Y, et al. Therapeutic trials in 200 patients with HTLV-I-associated myelopathy/tropical spastic paraparesis. J Neurovirol **2**: 345-355, 1996.
4. Nomoto M, Utatsu Y, Soejima Y, Osame M. Neopterin in cerebrospinal fluid: a useful marker for diagnosis of HTLV-I-associated myelopathy/tropical spastic paraparesis. Neurology **41**: 457, 1991.
5. Ali A, Rudge P, Dalgleish AG. Neopterin concentrations in serum and cerebrospinal fluid in HTLV-I infected individuals. J Neurol **239**: 270-272, 1992.
6. Ashkar S, Weber GF, Panoutsakopoulou V, et al. Eta-1 (osteopontin): an early component of type-1 (cell-mediated) immunity. Science **287**: 860-864, 2000.
7. Chabas D, Baranzini SE, Mitchell D, et al. The influence of the proinflammatory cytokine, osteopontin, on autoimmune demyelinating disease. Science **294**: 1731-1735, 2001.
8. Braitch M, Constantinescu CS. The role of osteopontin in experimental autoimmune encephalomyelitis (EAE) and multiple sclerosis (MS). Inflamm Allergy Drug Targets **9**: 249-256, 2010.
9. Nagai M, Yamano Y, Brennan MB, Mora CA, Jacobson S. Increased HTLV-I proviral load and preferential expansion of HTLV-I Tax-specific $CD8^+$ T cells in cerebrospinal fluid from patients with HAM/TSP. Ann Neurol **50**: 807-812, 2001.
10. Nagai M, Usuku K, Matsumoto W, et al. Analysis of HTLV-I proviral load in 202 HAM/TSP patients and 243 asymptomatic HTLV-I carriers: high proviral load strongly predisposes to HAM/TSP. J Neurovirol **4**: 586-593, 1998.
11. Matsuoka E, Takenouchi N, Hashimoto K, et al. Perivascular T cells are infected with HTLV-I in the spinal cord lesions with HTLV-I-associated myelopathy/tropical spastic paraparesis: double staining of immunohistochemistry and polymerase chain reaction in situ hybridization. Acta Neuropathol **96**: 340-346, 1998.
12. Umehara F, Izumo S, Nakagawa M, et al. Immunocytochemical analysis of the cellular infiltrate in the spinal cord lesions in HTLV-I-associated myelopathy. J Neuropathol Exp Neurol **52**: 424-430, 1993.
13. Umehara F, Izumo S, Ronquillo AT, Matsumuro K, Sato E, Osame M. Cytokine expression in the spinal cord lesions in HTLV-I-associated myelopathy. J Neuropathol Exp Neurol **53**: 72-77, 1994.
14. Nishimoto N, Yoshizaki K, Eiraku N, et al. Elevated levels of interleukin-6 in serum and cerebrospinal fluid of HTLV-I-associated myelopathy/tropical spastic paraparesis. J Neurol Sci **97**: 183-193, 1990.
15. Furuya T, Nakamura T, Fujimoto T, et al. Elevated levels of interleukin-12 and interferon-gamma in patients with human T lymphotropic virus type I-associated myelopathy. J Neuroimmunol **95**: 185-189, 1999.
16. Denhardt DT, Guo X. Osteopontin: a protein with diverse functions. FASEB J **7**: 1475-1482, 1993.
17. Braitch M, Nunan R, Niepel G, Edwards LJ, Constantinescu CS. Increased osteopontin levels in the cerebrospinal fluid of patients with multiple sclerosis. Arch Neurol **65**: 633-635, 2008.
18. Bornsen L, Khademi M, Olsson T, Sorensen PS, Sellebjerg F. Osteopontin concentrations are increased in cerebrospinal fluid during attacks of multiple sclerosis. Mult Scler **17**: 32-42, 2011.
19. Wen SR, Liu GJ, Feng RN, et al. Increased levels of IL-23 and osteopontin in serum and cerebrospinal fluid of multiple sclerosis patients. J Neuroimmunol **244**: 94-96, 2012.
20. Izumo S, Goto I, Itoyama Y, et al. Interferon-alpha is effective in HTLV-I-associated myelopathy: a multicenter, randomized, double-blind, controlled trial. Neurology **46**: 1016-1021, 1996.
21. Yamano Y, Sato T. Clinical pathophysiology of human T-lymphotropic virus-type 1-associated myelopathy/tropical spastic paraparesis. Front Microbiol **3**: 389, 2012.
22. Fuchs D, Stahl-Hennig C, Gruber A, et al. Neopterin: its clinical use in urinalysis. Kidney Int Suppl **47**: S8-S11, 1994.
23. Zhang J, Yamada O, Matsushita Y, et al. Transactivation of human osteopontin promoter by human T-cell leukemia virus type 1-encoded Tax protein. Leuk Res **34**: 763-768, 2010.
24. Alberti C, Cartier L, Valenzuela MA, Puente J, Tanaka Y, Ramirez E. Molecular and clinical effects of betamethasone in human T-cell lymphotropic virus type-I-associated myelopathy/tropical spastic paraparesis patients. J Med Virol **83**: 1641-1649, 2011.
25. Croda MG, de Oliveira AC, Vergara MP, et al. Corticosteroid therapy in TSP/HAM patients: the results from a 10 years open cohort. J Neurol Sci **269**: 133-137, 2008.

Journal of Neuroimmunology 254 (2013) 183–186

Contents lists available at SciVerse ScienceDirect

Journal of Neuroimmunology

journal homepage: www.elsevier.com/locate/jneuroim

Short communication

Antibodies against Wnt receptor of muscle-specific tyrosine kinase in myasthenia gravis

Masaharu Takamori [a,*], Tatsufumi Nakamura [b], Masakatsu Motomura [c]

[a] Neurological Center, Kanazawa-Nishi Hospital, 6-15-41, Ekinishi-Honmachi, Kanazawa, Ishikawa-ken 920-0025, Japan
[b] Department of Molecular Microbiology and Immunology, Graduate School of Biomedical Sciences, Nagasaki University, 1-12-4, Sakamoto, Nagasaki, Nagasaki-ken 852-8523, Japan
[c] Department of Internal Medicine, Graduate School of Biomedical Sciences, Nagasaki University, 1-7-1, Sakamoto, Nagasaki, Nagasaki-ken 852-8501, Japan

ARTICLE INFO

Article history:
Received 7 June 2012
Received in revised form 21 July 2012
Accepted 3 September 2012

Keywords:
Myasthenia gravis
Neuromuscular junction
Acetylcholine receptor
Muscle-specific tyrosine kinase
Wnt

ABSTRACT

Muscle-specific tyrosine kinase (MuSK) antibodies are detected in a proportion of myasthenia gravis (MG) patients who are negative for acetylcholine receptor (AChR) antibodies and have prominent bulbar weakness and crises. In the MuSK ectodomains, the immunoglobulin-like 1 and 2 domains (Ig1/2) mediate the agrin–Lrp4–MuSK signaling and the cysteine-rich domain (CRD) mediates the Wnt–MuSK–Dishevelled signaling; both contribute to AChR clustering. Immunoblotting against recombinant proteins showed MuSK Ig1/2 antibodies in 33 anti-AChR-negative MG patients; 10 patients of them (30%) were additionally positive for MuSK CRD antibodies. The result suggests that MuSK antibodies have heterogeneity in their binding to functional domains of MuSK.

1. Introduction

Myasthenia gravis (MG) is a disease of neuromuscular junction (NMJ) which is mainly caused by an immune response to the nicotinic acetylcholine receptor (AChR) in skeletal muscle. A proportion of MG patients are negative for AChR antibodies, and instead have antibodies (largely IgG4 and partially IgG1) against the muscle-specific tyrosine kinase (MuSK) (Vincent et al., 2008) with the clinical features including prevalence in women, prominent bulbar involvement, crises and anticholinesterase nonresponsiveness (Pasnoor et al., 2010; Guptill et al., 2011). MuSK is stimulated from "inside" the muscle cells by Dok7 (Yamanashi et al., 2012), and from the "outside" by Lrp4 (agrin receptor) with and without agrin (Weatherbee et al., 2006; Kim et al., 2008; Zhang et al., 2008); MuSK thereby contributes to AChR stabilization and clustering through various intracellular kinase cascades (Wu et al., 2010). Also, MuSK contains the receptor for Wnts which belong to a family of secreted glycoproteins and interact with the muscle-expressed Dishevelled (Dvl) that is essential for the noncanonical Wnt signaling cascade contributing to AChR clustering (Luo et al., 2002; Korkut and Budnik, 2009; Wu et al., 2010); this pathway also regulates a retrograde signaling to nerve terminals (Luo et al., 2002). In the MuSK ectodomains, its first and second immunoglobulin-like domains (Ig1/2) mediate the agrin–Lrp4 signaling (Stiegler et al., 2006) and its cysteine-rich domain (CRD) mediates the Wnt signaling (Stiegler et al., 2009). In view of these, we studied the MG patients focusing on the antibodies against the MuSK CRD in association with the antibodies against the MuSK Ig1/2 domains.

2. Patients and methods

2.1. Patients

Serum samples were obtained from 43 anti-AChR-negative patients, aged from 6 to 80 years at onset (13 men and 30 women), with generalized MG defined by the Myasthenia Gravis Foundation of America (MGFA) classification (grades from IIa to V) (Jaretzki et al., 2000). The diagnosis was based on fatigable muscle weakness with electrophysiological evidence of decrementing compound muscle action potentials to low-rate repetitive nerve stimulation or increased jitter on single-fiber electromyography; a positive response to edrophonium injection was considered as a finding in favor of the diagnosis. Thirty-three patients, aged from 6 to 80 years at onset (10 men and 23 women), of these 43 patients were positive for MuSK antibodies (ranged from 5.32 to 131.40 nM. control, <0.05 nM) determined by the standard radioimmunoassay (RIA) (McConville et al., 2004); the remaining 10 patients negative for standard RIA-determined MuSK antibodies, aged from 20 to 65 years at onset (3 men and 7 women) were also studied as MG diagnosed by clinical and electrophysiological features (MGFA-graded from IIa to IIIa). Control sera were obtained from 10 healthy volunteers aged from 22 to 43 years (5 men and 5 women) and from 10 disease controls with MG, aged from 18 to 70 years at onset (2 men

* Corresponding author. Tel.: +81 76 233 1811; fax: +81 76 221 8603.
E-mail address: m-takamori@vanilla.ocn.ne.jp (M. Takamori).

0165-5728/$ – see front matter © 2012 Elsevier B.V. All rights reserved.
http://dx.doi.org/10.1016/j.jneuroim.2012.09.001

and 8 women) and MGFA-graded from IIb to IIIb who were positive for AChR antibodies (from 5.6 to 77.0 nM. control, <0.2 nM) and negative for standard RIA-determined MuSK antibodies (<0.05 nM).

2.2. Recombinant expression of MuSK Ig1/2 domains and CRD

DNA fragments coding from human MuSK Ig1/2 domain-contained amino acid residues (22–212) (Stiegler et al., 2006) and CRD-contained amino acid residues (313–494) (Stiegler et al., 2009) were generated by PCR method using human MuSK cDNA (OriGene Technol., USA) as a template. Expression constructs were generated in pcDNA3.3-TOPO (Invitrogen, USA) with DNA fragments ligated to the synthetic mouse trypsin prepro sequence followed by 7 histidines tagged at the N-terminus. Human embryonic kidney (HEK) 293F cells (Invitrogen, USA) were transiently transfected with these constructs according to the instructions (FreeStyle™293 Expression System, Invitrogen, USA), and the cultured supernatants were harvested for 4 days after transfection. Clarified supernatants were directly loaded onto a HisTrap HP column (GE Healthcare, USA) equilibrated with 0.1 M Tris–Cl, 0.5 M NaCl, 20 mM Imidazole, pH 7.4. After the column was washed with the equilibration buffer, Ig1/2 and CRD proteins were eluted with linear gradient of Imidazole. Purity of Ig1/2 and CRD proteins was analyzed by sodium dodecyl sulfate-polyacrylamide gel electrophoresis (SDS-PAGE) (Invitrogen, USA) and Western blotting using mouse anti-human monoclonal antibodies (ab86456 for Ig1/2 and ab55549 for CRD. Abcam, USA).

2.3. Western blot analysis

Either Ig1/2 domains or CRD of MuSK at an amount of 5 μg/lane was subjected to 12.5% SDS-PAGE under reducing conditions with dithiothreitol. Proteins were transfected onto a polyvinylidene difluoride membrane and were then cut into strips. The antibody detection was performed by using Immun-Blot® Assay Kit (Bio-Rad Lab., USA). In brief, after blocking with Tris buffered saline containing 3% gelatin for 1 h, each strip was incubated with the serum sample which was diluted from 1:100 to 1:1000 and with a 1000-fold-diluted each mouse anti-human monoclonal antibody (used for the confirmation of purified recombinant protein) at room temperature for 1 h. After 30 min-incubation with 3000-fold-diluted goat anti-human IgG or anti-mouse IgG conjugated with alkaline phosphatase (AP), specific reactivity was estimated by the intensity with which each strip was stained with AP color development solution. The 22 kDa and 38 kDa immunostained bands were visualized for MuSK Ig1/2 and CRD monoclonal antibodies, respectively. When the serum sample showed the immunostained band at the same migration position as that proved with the test monoclonal antibody in the serum dilutions more than 1:500, the result was judged as antibody-positive.

3. Results

In the study collecting the serum samples from 43 anti-AChR-negative MG patients, 10 patients were negative for MuSK antibodies determined by both the standard RIA and the present study (group 3 in Table 1). All of the remaining 33 patients positive for MuSK antibodies determined by RIA were positive for MuSK Ig1/2 antibodies (groups 1 and 2 in Table 1); 10 patients of them (30%) were additionally positive for MuSK CRD antibodies (group 1 in Table 1). None was positive for MuSK CRD antibodies alone. Ten disease controls (anti-AChR-positive MG; group 4 in Table 1) and 10 healthy volunteers were all negative for MuSK Ig1/2 and MuSK CRD antibodies as well as for standard RIA-determined MuSK antibodies. The disease severity (MGFA grades) and clinical symptoms in each group showed that a trend was noted toward severe severity in anti-MuSK-positive MG (groups 1 and 2 in Table 1). However, there was no significant correlation between the positive (group 1 in Table 1)/negative (group 2 in Table 1) results from MuSK CRD antibody determination and the MGFA grades (Wilcoxon test, $p = 0.0747$). Representative immunoblots are shown in Fig. 1: C corresponding to group 1 and D corresponding to group 2 in Table 1. No immunostained band for MuSK Ig1/2 and MuSK CRD was seen with the serum from an anti-AChR-positive MG patient (B corresponding to group 4 in Table 1). The antibody specificity was confirmed by the same migration positions as those of purified, CBB-stained recombinant proteins (A in Fig. 1).

Table 1
Clinical and immunological profiles of 53 myasthenia gravis (MG) patients.

Groups (numbers of patients)	1 (10)	2 (23)	3 (10)	4 (10)
Age at onset (years)	22–75	6–80	20–65	18–70
Gender	F 8/M 2	F 15/M 8	F 7/M 3	F 8/M 2
Antibodies against				
• MuSK Ig1/2 domains (immunoblot)	Positive	Positive	Negative	Negative
• MuSK CRD (immunoblot)	Positive	Negative	Negative	Negative
• Full-length of MuSK extracellular segment, determined by standard RIA (control, <0.05 nM)	6.08–131.40 nM	5.32–45.75 nM	<0.05 nM	<0.05 nM
• AChR, determined by standard RIA (control, <0.2 nM)	<0.2 nM	<0.2 nM	<0.2 nM	5.6–77.0 nM
MG severity (MGFA grades)				
IIa	0	3	4	0
IIb	0	7	2	3
IIIa	0	2	4	6
IIIb	4	1	0	1
IVa	0	0	0	0
IVb	0	0	0	0
V	6	10	0	0
Clinical symptoms				
Facial/bulbar weakness	10	20	2	4
Respiratory crisis	5	10	0	0
Neck weakness	5	2	0	0
Ophthalmoplegia	9	21	10	10
Limb weakness	6	13	10	7

F: female. M: male. MuSK: muscle-specific tyrosine kinase (Ig1/2 domains: immunoglobulin-like 1 and 2 domains; CRD: cysteine-rich domain). AChR: acetylcholine receptor. RIA: radioimmunoassay. MGFA: Myasthenia Gravis Foundation of America. Figures in MG severity and clinical symptoms indicate numbers of the patients subject to each item.

4. Discussion

This brief report shows that MuSK antibodies in a part of MG patients recognize not only the main immunogenic site(s) (Ig1/2 domains) responsible for the agrin signaling (McConville et al., 2004) but also the CRD responsible for the Wnt signaling (Stiegler et al., 2009). However, it remains to study as to whether the antibody heterogeneity could correlate with disease activity or characteristics.

Recent studies highlight Wnt involvement in critical aspects of the NMJ function and structure (Korkut and Budnik, 2009; Wu et al., 2010). Wnts 11 (Jing et al., 2009; Zhang et al., 2012), 9a (Zhang et al., 2012), 4 (Strochlic et al., 2012) and 3 (Henriquez et al., 2008), which are released from neurons or derived from muscles, bind to MuSK CRD and contribute to the AChR clustering via the Dvl-mediated noncanonical Wnt signaling cascade (Luo et al., 2002; Korkut and Budnik, 2009; Wu et al., 2010; Zhang et al., 2012). Therefore, the Wnt–Dvl signaling via MuSK CRD converges upon the agrin–Lrp4 signaling via MuSK Ig1/2 domains, and both contribute to AChR clustering. Therefore, our results suggest that MuSK CRD antibodies could be involved in impairment of the Wnt–MuSK interaction, suggesting a diversity to MuSK-implicated pathophysiology in MG.

Reportedly, the inhibited MuSK–Dvl interaction decreases the frequency of spontaneous synaptic currents (SSC) in association

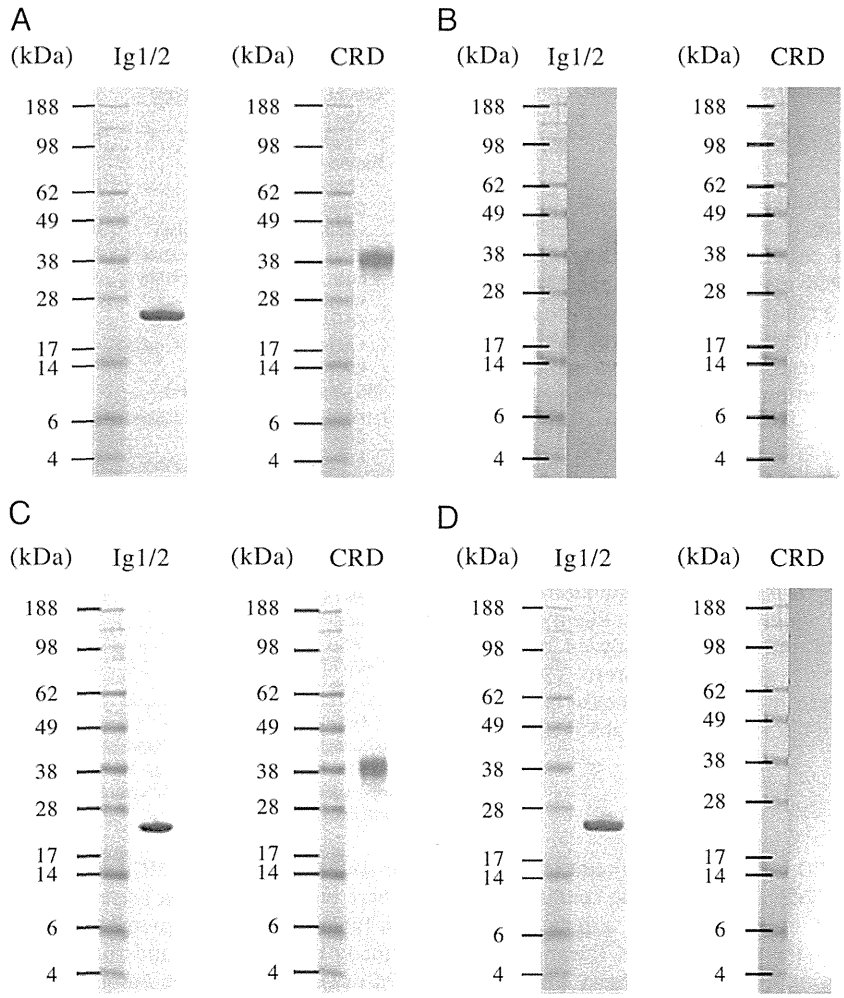

Fig. 1. Immunoblots of purified recombinant proteins of human MuSK extracellular segment (Ig1/2: immunoglobulin-like 1 and 2 domains; CRD: cysteine-rich domain) and immunostained reactivity with serum samples (1:500 dilution) from myasthenia gravis patients at 5 μg of recombinant protein/lane. A: Identification of purified, CBB-stained recombinant proteins (Ig1/2 domains: 1250 ng/lane; CRD: 2240 ng/lane). B: No reactivity was found for Ig1/2 domains and CRD with the serum from a 58 year-old man who was positive for AChR antibodies (9.8 nM), negative for MuSK antibodies (<0.05 nM) and MGFA-graded IIIb. C: Reactivity was found positive for both Ig1/2 domains and CRD with the serum from a 78 year-old woman who was negative for AChR antibodies (<0.2 nM), positive for MuSK antibodies (131.40 nM) and MGFA-graded V. D: Reactivity was found positive for Ig1/2 domains but negative for CRD with the serum from a 72 year-old man who was negative for AChR antibodies (<0.2 nM), positive for MuSK antibodies (45.75 nM) and MGFA-graded V. MuSK antibody titers shown in the parentheses were determined by the standard radioimmunoassay (RIA) (control,<0.05 nM). AChR antibody titers in the parentheses were also determined by conventional RIA (control, <0.2 nM).

with the decreased SSC amplitude in the NMJ, suggesting a defect in ACh release upregulation which may reflect retrograde Wnt signaling at the nerve terminal (Luo et al., 2002). The antibody-induced disturbance in bidirectional Wnt signaling via MuSK may, at least in part, be compatible with presynaptic abnormalities including the absence of ACh release upregulation to compensate for postsynaptic failure found in anti-MuSK-positive MG patients (Niks et al., 2010) and animal models (Cole et al., 2008; Richman et al., 2011; Klooster et al., 2012; Mori et al., 2012; Viegas et al., 2012).

We demonstrated that MuSK antibodies have heterogeneity in their binding to functional domains of MuSK. However, the present results cannot be informative to the significant difference in disease activity in MG patients who are MuSK Ig1/2 antibody-positive versus MuSK Ig1/2 and CRD antibody-positive. To establish the significance of MuSK CRD antibody specificity, the future studies need to include larger numbers of well-characterized patients, cell-based antibody assay, and passive and active immunization models.

Acknowledgments

The authors declare no conflicts of interest.

References

Cole, R.N., Reddel, S.W., Gervásio, O.L., Phillips, W.D., 2008. Anti-MuSK patient antibodies disrupt the mouse neuromuscular junction. Ann. Neurol. 63, 782–789.
Guptill, J.T., Sanders, D.B., Evoli, A., 2011. Anti-MuSK antibody myasthenia gravis: clinical findings and response to treatment in two large cohorts. Muscle Nerve 44, 36–40.
Henriquez, P.P., Webb, A., Bence, M., Bildsoe, H., Sahores, M., Hughes, S.M., Salinas, P.C., 2008. Wnt signaling promotes AChR aggregation at the neuromuscular synapse in collaboration with agrin. Proc. Natl. Acad. Sci. U. S. A. 105, 18812–18817.
Jaretzki III, A., Barohn, R.J., Ernstoff, R.M., Kaminski, H.L., Keesey, J.C., Penn, A.S., Sanders, D.B., 2000. Myasthenia gravis: recommendations for clinical research standards. Task Force of the Medical Scientific Advisory Board of the Myasthenia Gravis Foundation of America. Neurology 55, 16–23.
Jing, L., Lefebvre, J.L., Gordon, L.R., Granato, M., 2009. Wnt signals organize synaptic prepattern and axon guidance through the zebrafish unplugged/MuSK receptor. Neuron 61, 721–733.
Kim, N., Stiegler, A.L., Cameron, T.O., Hallock, P.T., Gomez, A.M., Huang, J.H., Hubbard, S.R., Dustin, M.L., Burden, S.J., 2008. Lrp4 is a receptor for agrin and forms a complex with MuSK. Cell 135, 334–342.
Klooster, R., Plomp, J.J., Huijbers, M.G., Niks, E.H., Straasheijm, K.R., Detmers, F.J., Hermans, P.W., Sleijpen, K., Verrips, A., Losen, M., Martinez-Martinez, P., De Baets, M.H., van der Maarel, S.M., Verschuuren, J.J., 2012. Muscle-specific kinase myasthenia gravis IgG4 autoantibodies cause severe neuromuscular junction dysfunction in mice. Brain 135, 1081–1101.
Korkut, C., Budnik, V., 2009. Wnts tune up the neuromuscular junction. Nat. Rev. 10, 627–634.
Luo, Z.G., Wang, Q., Zhou, J.Z., Wang, J., Luo, Z., Liu, M., He, X., Wynshaw-Boris, A., Xiong, W.C., Lu, B., Mei, L., 2002. Regulation of AChR clustering by Dishevelled interacting with MuSK and PAK1. Neuron 35, 489–505.